New Mechanics-Based Confinement Model and Stress-Strain Relationship for Analysis and Design of Concrete Columns Wrapped with FRP Composites

Koosha Khorramian[1] and Pedram Sadeghian[2]

ABSTRACT: The analysis and design of concrete columns wrapped with fiber-reinforced polymer (FRP) composites require the mathematical equation of stress-strain relationship and the ultimate conditions (i.e., stress and strain) corresponding to the failure of FRP-confined concrete. The ultimate conditions of FRP-confined concrete were mostly developed using empirical methods based on regression analysis of test data obtained from the literature. There is a lack of mechanics-based formulations of the ultimate condition. In addition, from a practical design perspective, despite new advancements in the field of FRP confinement and the availability of sophisticated analysis-oriented and data-driven models, design guidelines and practicing engineers mainly need a single equation for the stress-strain relationship of confined concrete. Thus, in this study, a five-parameter William-Warnke plasticity model was utilized to find a new mechanics-based prediction of the ultimate condition of FRP-confined concrete using an updated database of 788 test data. Moreover, a new optimized stress-strain relationship based on the general expression of the Richard and Abbott equation was developed using 200 complete experimental stress-strain curves from 16 different independent studies. The proposed stress-strain relationship was presented in a single equation for the ease of application and its performance was verified against the experimental curves.

[1] PhD Candidate, Department of Civil and Resource Engineering, Dalhousie University, D301, 1360 Barrington street, Halifax, NS, B3H 4R2 Canada, Koosha.Khorramian@dal.ca

[2] Associate Professor and Canada Research Chair in Sustainable Infrastructure, Department of Civil and Resource Engineering, Dalhousie University, D401, 1360 Barrington Street, Halifax, NS, B3H 4R2 Canada, Pedram.Sadeghian@dal.ca (corresponding author)

1. INTRODUCTION

It has been almost four decades that FRP-confined concrete columns are being continuously investigated by researchers and various predictions of the stress-strain curves and the ultimate condition is being updated. Recent studies showed that the finite element modeling (FEM) of the FRP-confined concrete is in very good agreement with the experimental tests [1–4]. The requirement for accurate FEM is precise plasticity-based failure criteria and damage models. Thus, many researchers focused on the development of characteristics of failure surfaces of FRP-confined concrete columns using Mohr-Coulomb criterion [5,6] and Drucker-Prager failure criterion [7–9] as well as developing damage models [10–12]. The latter shows the importance of plasticity-based modeling, which can be incorporated into the prediction of ultimate confined strength of FRP-confined concrete column. The literature showed that only a few studies considered a plasticity-based approach to develop estimation for the ultimate confined strength [13–18], while most of the available models were empirically developed using a variety of regression techniques [19–28]. Mander et al. [13] developed a model to predict the strength of the concrete confined by steel reinforcement using a five-parameter Willam-Warnke model [29] which was later improved by Bing et al. [14] for transverse steel. Later, Afifi et al. [15] and Hales et al. [16] studied confinement of FRP ties and spirals. Yan et al. [18], calibrated the model for FRP-wrapped concrete columns. However, the test data used for the calibration was limited (i.e., less than 20 data points), and further study is required using more comprehensive and recent database. Recently, an updated database of 788 FRP-confined concrete columns is available in the literature [26,30]. Therefore, there is a gap in the assessment of the ultimate confined strength using a mechanics-based model which engages the most recent FRP-confined column database. Recently, more sophisticated methods such as using artificial intelligence (AI) [31,32] and extensive

numerical models [33,34] were developed to predict the ultimate condition. However, for design and analysis purposes, simplified design-oriented models are the most practical because of their simplicity, accuracy, and ease of use. The same concept applies to the stress-strain curves, since many analysis-oriented models predict the FRP-confined concrete strength [35–43], while the design guidelines [44,45], and in turn practice engineers, use the design-oriented models for analysis and design purposes. Thus, this study proposes a simplified design-oriented stress-strain relationship for FRP-confined concrete columns using actual FRP-confined stress-strain curves. It should be noted that the current study utilizes the mechanics based approach and does not cover the concrete strength affected by the stress-path dependence of confinement [108-110] as well as the details of concrete microstructures, which would affect the splitting crack onset of core concrete [111-112]. The latter is out of the scope of this study.

In 1982, Fardis and Khalili [46], proposed a design-oriented model to predict the axial stress-strain curve of FRP-confined concrete columns. The model was adopted for actively confined concrete columns or the ones confined with steel tubes which expressed in form of a single parabolic curve, whose accuracy was later improved by other researchers [47–49]. The problem with a single parabolic stress-strain model, which mainly is based on the model proposed by Popovics [50], is that these curves do not accurately predict the bilinear form of the stress-strain curves for FRP-confined concrete columns as observed in the experimental tests. Thus, many researchers used the bilinear stress-strain curves to distinguish the FRP-confined concrete behavior from steel confined concrete columns [51–55]. These curves consisted of two lines defined by three points including the origin, a transition point close to the location of the unconfined concrete strength, and the point corresponding to the ultimate condition. However, the problem is that the

unconfined concrete and confined concrete showed similar behavior in the initial ascending branch of the stress-strain curves for low levels of concrete dilation where the confinement is not activated.

Therefore, in the recent studies, an improved version of the stress-strain curve for FRP-confined columns was developed which shows an initial parabolic curve followed by a linear part. Some researchers have adopted the parabolic part proposed by Hognestad [56] as the initial part followed by a secondary linear portion that connects the transition point to the point corresponding to the ultimate condition [57–60], while Lam and Teng developed a new prediction for the initial portion [25] which was adopted by other researchers [24,61–64]. In form of a single equation, a model was proposed by Toutanji [65] based on a general expression developed by Sargin [66] and improved by Ahmad and Shah [67] for steel tubes, which was adopted by researchers [22,68]. The other popular format of the confined concrete stress-strain curve with one single power equation is the general expression proposed by Richard and Abbott [69] which required four parameters (i.e. the slope of the initial ascending branch, the secondary slope, the intercept of secondary slope and the stress axis, and a polynomial constant which determine the smoothness of transition), which was adopted by many researchers [21,70–75].

Most of the mentioned models relate the secondary slope of the stress-strain curve to the ultimate condition and the intercept of the secondary line with the stress axis. However, the ultimate condition is related to the rupture strain of FRP wraps which showed a high variability [76–78]. Chen et al. [78] studied the factors affecting the variability in the ultimate condition based on an extensive literature survey and found that rupture of FRP may occur near the outer part, inner part, or outside of the overlap if FRP rupture controls the failure, and mixed debonding and rupture of FRPs may be the cause of the failure which may start at the middle of the column or near the ends of the columns. It was also found that seventeen factors may affect the FRP rupture

[78] that directly related to the ultimate confined strength and strain. The latter showed that the secondary slope of the stress-strain of the FRP-confined concrete may experience errors by involving the ultimate condition. However, only a few stress-strain curves are available in the literature which consider the secondary slope to the FRP wrap properties and unconfined concrete strength instead of the ultimate condition [21,63,64,70]. Fahmy et al. [63] adopted the model developed by Lam and Teng [25] and improved the model by relating the secondary slope. However, the intercept stress was kept constant as the unconfined concrete. Samman et al. [21] used only 30 specimens for calibration of the model. Xiao and Wu [70] incorporate an analysis-oriented approach and verified their model versus an experimental database. Bai et al. [64] proposed a model for large rupture strain FRP-confined concrete.

Therefore, in the current study, a stress-strain curve was proposed by adopting a four-parameter Richard and Abbott [69] general expression, which is a single equation, using 200 full stress-strain curves from sixteen independent studies included 130 carbon, 22 aramid, 42 glass, and 6 basalt FRP-wrapped concrete columns. The curve parameters were determined independent of the ultimate condition and the intercept stress was considered as a variable. Also, the accuracy of the curves was evaluated using a total of 3272 data points from the experimental curves comparing to fifteen other studies. In the end, based on the stress-stain curve and the proposed plasticity-based confined strength equation, a prediction of ultimate confined strain was given.

2. CALIBRATION OF WILLAM-WARNKE MODEL FOR ULTIMATE STRENGTH

To obtain a relationship for predicting the ultimate strength of concrete columns confined with FRP wraps, the five parameter Willam-Warnke plasticity model was used [29]. This plasticity model describes the failure surface in principal stress space (σ_1, σ_2, σ_3). The failure surface can be

expressed in terms of octahedral normal stress (σ_{oct}) and octahedral shear stress (τ_{oct}) as presented in Eq. 1 and 2.

$$\sigma_{oct} = \frac{1}{3}(\sigma_1 + \sigma_2 + \sigma_3) \tag{1}$$

$$\tau_{oct} = \frac{1}{3}\sqrt{[(\sigma_1 - \sigma_2)^2 + (\sigma_1 - \sigma_3)^2 + (\sigma_2 - \sigma_3)^2]} \tag{2}$$

Fig. 1(a) shows the schematic interpretation of the five parameter Willam-Warnke failure surface in ξ-r-θ coordinate system; where ξ is the norm of projection of stress state on the hydrostatic axis ($\sigma_1 = \sigma_2 = \sigma_3$); r is the norm of projection of stress state on a deviatoric plane which is a plane perpendicular to the hydrostatic axis ($\sigma_1 + \sigma_2 + \sigma_3 = constant$); θ is the angle of similarity which is the angle between stress state point ($\sigma_1, \sigma_2, \sigma_3$) and the projection of σ_1 axis in its deviatoric plane, as presented in Fig. 1(b). The octahedral normal and shear stresses are directly proportional to ξ and r, respectively, as shown in Fig. 1(a). The angle of similarity is defined in Eq. 3 where S_1 is the deviatoric principal stress corresponding to σ_1, J_2 is the second invariant of the deviatoric stress tensor, and $\sigma_1, \sigma_2, \sigma_3$ are the principal stresses [79].

$$\theta = \frac{\sqrt{3}}{2}\frac{S_1}{\sqrt{J_2}} = \frac{2\sigma_1 - \sigma_2 - \sigma_3}{2\sqrt{3}\sqrt{\frac{1}{6}[(\sigma_1 - \sigma_2)^2 + (\sigma_1 - \sigma_3)^2 + (\sigma_2 - \sigma_3)^2]}} \tag{3}$$

When two of the principal stresses are the same, the compression meridian ($\sigma_3 < \sigma_1 = \sigma_2$) and tensile meridian ($\sigma_2 = \sigma_3 < \sigma_1$) can be derived. Meridians are the intersection of the failure surface and the meridian plane which contains the hydrostatic axis with a constant angle of similarity (θ). It should be noted that the sign convention was defined so that tensile stresses are positive and compressive stresses are negative. By substituting the mentioned condition in Eq. 3, angles of similarity of 60 and 0 degrees are derived for compression meridian and tensile meridians, respectively, as shown in Fig. 1(a). In Willam-Warnke five parameter model, the tensile

and compression meridians are in parabolic form as shown in Fig. 2 and expressed in Eq. 4 and 5, respectively [29].

$$\bar{\tau}_{oct-T} = a_0 + a_1 \bar{\sigma}_{oct-T} + a_2 \bar{\sigma}_{oct-T}^2 \tag{4}$$

$$\bar{\tau}_{oct-C} = b_0 + b_1 \bar{\sigma}_{oct-C} + b_2 \bar{\sigma}_{oct-C}^2 \tag{5}$$

Eqs.4 and 5 are expressed in terms of octahedral stresses normalized with the unconfined concrete strength (f'_{co}) and parameters a_0, a_1, a_2, b_0, b_1, b_2 are constants. The index T appears for tensile meridian, the index C appears for compression meridian, $\bar{\sigma}_{oct}$ is the normalized octahedral stress, and $\bar{\tau}_{oct}$ is the normalized octahedral shear stress which are presented in Eq. 6.

$$\bar{\sigma}_{oct} = \frac{\sigma_{oct}}{f'_{co}} \quad ; \quad \bar{\tau}_{oct} = \frac{\tau_{oct}}{f'_{co}} \tag{6}$$

In this study, a database including concrete specimens wrapped with FRP and tested under pure compression was used to find the strength model. The database includes 778 tests of confined concrete columns collected by Sadeghian and Fam [26] and expanded by Khorramian [30]. The summary of the database is presented in Table 1. For all points in the database, the ultimate confining pressure (f_l) was calculated based on Eq. 7 in which D is the diameter of concrete columns, E_f and t_f are the modulus of elasticity and the thickness of FRP wraps, respectively, and ε_{hr} is the actual hoop rupture strain of the wraps in the compression test of columns.

$$f_l = \frac{2E_f t_f \varepsilon_{hr}}{D} \tag{7}$$

Fig. 3 shows the state of stress for the compressive tests in which the ultimate confining pressure (f'_{cc}) is greater than axisymmetric confining pressure (f_l). Therefore, the state of stress for tests and their relationship with principal stresses can be explained in Eq. 8.

$$\sigma_3 = -f'_{cc} \quad ; \quad \sigma_1 = \sigma_2 = -f_l \quad ; \quad \left| f'_{cc} \right| \geq |f_l| \quad ; \quad \sigma_3 \leq \sigma_1 = \sigma_2 \tag{8}$$

The state of stress for the confined concrete tests is the same as the compressive meridian explained earlier, and each experimental test represents a point on the compression meridian in the octahedral space. Each set of (f'_{cc}, f_l) was transformed into an octahedral set of ($\bar{\sigma}_{oct}$, $\bar{\tau}_{oct}$) by substituting the stress state from Eq.8 into Eq. 1, 2, and 6 which leads to Eq. 9 and 10.

$$\bar{\sigma}_{oct} = \frac{-(f'_{cc} + 2f_l)}{3f'_{co}} \tag{9}$$

$$\bar{\tau}_{oct} = \frac{\sqrt{2}(f'_{cc} - f_l)}{3f'_{co}} \tag{10}$$

Fig. 4 shows the database in the normalized octahedral stress space to which a parabolic equation was fitted. The root mean squared error (RMSE) for the fitted equation is 0.0993 and the coefficient of determination (R^2) is not very close to one (i.e. 0.87) which is quite reasonable and shows a very good degree of accuracy. By comparing Eq. 5 with the fitted equation in the figure, three constants of compression meridian can be found ($b_0 = 0.1546$, $b_1 = 0.8293$, and $b_2 = -0.0750$), and the results lead to Eq. 11 that presents the compression meridian of confined concrete.

$$\bar{\tau}_{oct-C} = +0.1546 - 0.8293\bar{\sigma}_{oct-C} - 0.0750\bar{\sigma}^2_{oct-C} \tag{11}$$

To predict the ultimate confined concrete strength (f'_{cc}) from the ultimate confining pressure (f_l) and unconfined concrete strength (f'_{co}), Eqs. 9 and 10 were substituted in Eq. 5 that led to Eq. 12, and it was simplified and rearranged in the form of Eq. 13.

$$\frac{\sqrt{2}(f'_{cc} - f_l)}{3f'_{co}} = b_0 - b_1 \frac{(f'_{cc} + 2f_l)}{3f'_{co}} + b_2 \left(\frac{(f'_{cc} + 2f_l)}{3f'_{co}}\right)^2 \tag{12}$$

$$\frac{f'_{cc}}{f'_{co}} = \frac{3(b_1 + \sqrt{2})}{2b_2} + \sqrt{\left[\frac{3(b_1 + \sqrt{2})}{2b_2}\right]^2 - \frac{9b_0}{b_2} - \frac{9\sqrt{2}}{b_2}\frac{f_l}{f'_{co}} - 2\frac{f_l}{f'_{co}}} \tag{13}$$

By substituting the constants of the compressive meridian parabola from Eq. 11 into Eq.13, the strength ratio of confined concrete can be presented in the form of Eq. 14.

$$\frac{f'_{cc}}{f'_{co}} = -11.702 + 12.470 \sqrt{1 + 1.092\frac{f_l}{f'_{co}} - 2\frac{f_l}{f'_{co}}} \tag{14}$$

It should be noted that for analysis purposes, it is conventional to satisfy the boundary condition which shows equal confined and unconfined strength in the absence of the confining pressure. Thus, Eq. 15 was adjusted by keeping the format of Eq. 14 and minimizing the RMSE error for the experimental database to satisfy the boundary condition which required the same confined and unconfined strength in absence of confinement.

$$\frac{f'_{cc}}{f'_{co}} = -11.702 + 12.702 \sqrt{1 + 0.935\frac{f_l}{f'_{co}} - 2\frac{f_l}{f'_{co}}} \tag{15}$$

3. PERFORMANCE OF THE NEW ULTIMATE CONFINED STRENGTH MODEL

In order to evaluate the performance of the new ultimate confined strength model, a group of well-known plasticity-based and empirical models were selected from the literature and their performance was compared with the performance of the new model. The relationship between the ultimate confined concrete strength and the confining pressure can be written down in the form of Eqs. 16 and 17.

$$\frac{f'_{cc}}{f'_{co}} = A + \sqrt{A^2 - B - C\frac{f_l}{f'_{co}} - 2\frac{f_l}{f'_{co}}} \quad \rightarrow \quad \frac{f'_{cc}}{f'_{co}} = A + \lambda \sqrt{1 + \gamma\frac{f_l}{f'_{co}} - 2\frac{f_l}{f'_{co}}} \tag{16}$$

$$C = -\gamma\lambda^2 \ ; \ B = A^2 - \lambda^2 \tag{17}$$

By setting Eq. 16 equal to Eq. 13 and simplifying, the constants required for deriving the compression meridian (Eq. 5) can be found as presented in Eq. 18.

$$b_0 = \frac{b_2 B}{9} \ ; \ b_1 = \frac{2Ab_2}{3} - \sqrt{2}; \ b_2 = \frac{9\sqrt{2}}{C} \tag{18}$$

A comparison in the octahedral space was performed using five different formulas derived based on the Willam-Warnke failure surface as presented in Table 2. Mander et al. [13] developed a model for confined concrete columns confined by steel spirals and hoops using experimental test data and the explained procedure. Bing et al. [14] proposed an equation for high-strength concrete columns reinforced with transverse steel. Afifi et al. [15] and Hales et al. [16] for columns reinforced transversely with FRP spirals and hoops. For FRP wrapped columns, the only formula available in the literature which derived the ultimate confined strength based on the Willam-Warnke failure surface is a study performed by Yan et al. [18] in 2006, which was derived based on limited test data (less than 20 data points). For comparing the available equations, the root mean square error (RMSE) and average absolute error (AAE) were calculated using Eq. 19 and Eq. 20, respectively, where Exp_i is the ith experimental test data, $Calc_i$ is the ith calculated value from a predicting equation, and N is the total number of data points.

$$RMSE = \sqrt{\frac{\sum(Exp._i - Calc._i)^2}{N}} \tag{19}$$

$$AAE = \frac{\sum \left| \frac{Calc._i - Exp._i}{Exp._i} \right|}{N} \tag{20}$$

Table 2 shows that Eq. 11 gives the best estimation for the database in the octahedral space between the equations developed using the Willam-Warnke failure surface. Table 3 shows the format of the equations which predict the ultimate confined strength. The results of the comparison showed the lowest error for Eq. 14 and Eq. 15 developed in the current study.

To compare the proposed formula with empirical (non-plasticity-based) formulas for the prediction of ultimate confined strength, different formats of design-oriented equations were

presented in Table 4 and their error was calculated for the database. The results showed that the formulas developed by Sadeghian and Fam [26] and Lam and Teng [25] presented the lowest error to predict the ultimate confined strength whose error is comparable to Eq. 14 and Eq. 15. Fig. 5 shows the experimental versus model for the models developed in the current study and some of the models available in the literature. The results showed that the new models improved the current plasticity-based predictions and they are very close to non-plasticity-based models.

Fig. 6 presents a comparison of the database and different confinement models by showing the normalized confined concrete strength (f'_{cc}/f'_{co}) versus the normalized confining pressure (f_l/f'_{co}). Fig. 6(a) showed as the normalized confining pressure increases, some of the models underpredict the confined concrete strength (i.e. Mander et al. [13] and Sadeghian and Fam [26] models), while the developed models are in good alignment with the trend of the database. Also, Fig. 6(a) showed that the data points are concentrated up to a range of 0.6 for the formalized confining pressure (f_l/f'_{co}). Thus, in Fig. 6(b), the selected range of normalized confining pressure is presented, and the data points are removed for comparison. The proposed model by Mander et al. [13] overpredicts the confining strength while the one proposed by Yan et al. [18] underpredicts and then overpredicts the confined concrete strength. Other models showed almost similar behavior up to a normalized confining pressure of 1. However, for normalized confining pressures between 1 to 2, the proposed equations proposed by Lam and Teng [25] and Teng et al. [24] overpredict the confinement effect.

Eq. 14, which is developed which is the best fit for the failure surface in the octahedral space, showed that a minimum confining pressure is required so that the confined and unconfined concrete strength become equal which is called the confinement limit. To find the confinement limit Eq. 16 and 17 which show the general form of the ultimate confined strength is rewritten in

the form of Eqs. 21 and 22 to show the equation for the confining pressure given the ultimate confined strength.

$$\frac{f_l}{f'_{co}} = L - M\sqrt{1 + N\frac{f'_{cc}}{f'_{co}} - \frac{1}{2}\frac{f'_{cc}}{f'_{co}}} \tag{21}$$

$$L = \frac{A}{2} + \frac{1}{8}\lambda^2\gamma \ ; \ M = \sqrt{\frac{1}{8}\lambda^2\gamma A + \frac{1}{4}\left[\left(\frac{1}{4}\lambda^2\gamma\right)^2 + \lambda^2\right]} \ ; \ N = -\frac{\frac{1}{8}\lambda^2\gamma}{M^2} \tag{22}$$

By substituting the values from Eq. 14 into Eq. 21 and 22, the confining pressure can be presented in the form presented in Eq. 23.

$$\frac{f_l}{f'_{co}} = 15.369 - 15.519\sqrt{1 - 0.0881\frac{f'_{cc}}{f'_{co}} - \frac{1}{2}\frac{f'_{cc}}{f'_{co}}} \tag{23}$$

The relationship between the normalized confining pressure and normalized confined strength found in Eq. 23, can be used to determine the confinement limit, which is considered as the minimum confinement required to activate the unconfined concrete. To find the confinement limit, the value of normalized confined strength was set to one in Eq. 23 which gave a confinement limit of 0.05. It should be noted that ACI 440.2R [44] which adopted the proposed model by Lam and Teng [25], proposed a confinement limit of 0.08. for a better presentation of the limit and the database, Fig. 7(a) shows a reduced database including 200 data points used for further studies in the next section. It should be mentioned that only one data point was below the normalized confining limit of 0.05 while four of them were below the 0.08 limit in the reduced database. For all data points, 33 and 65 specimens experienced a normalized confining pressure less than 0.05 and 0.08, respectively. Therefore, the limit of 0.08 is more conservative although 0.05 represents the limit more accurately. Fig. 7(b) compares Eq. 14 and Lam and Teng [25] which revealed that the Lam and Teng model overpredicts the ultimate confined pressure up to a normalized confining

pressure limit of 0.2. The statistics from the database showed that 38% of the tested specimen (i.e. 302 out of 778) had a normalized confining pressure of less than 0.2. Thus, the overprediction leads to unconservative designs per ACI 440.2R [44] for a confining range up to 0.2. An alternative path is suggested by this study to cover the mentioned issues, shown as a dashed red line in Fig. 7(b). The suggestion is to neglect the effect of confinement on the strength up to normalized confining pressures below 0.05 (i.e. $f'_{cc}/f'_{co} = 1$ if $f_l/f'_{co} < 0.05$). Also, Eq. 14 can be used for the normalized confining pressures greater than 0.08. It should be mentioned that Fig. 6(a) showed that for the normalized confining pressures greater than 1, Lam and Teng [25] and in turn ACI 440.2R [44] are not conservative as many data points have lower confined concrete strength than their predicted values. Thus, for the mentioned range, the use of Eq. 14 is suggested in this study.

4. STRESS-STRAIN MODEL

This study presents a design-oriented stress-strain curve for FRP-confined concrete columns with only the ascending branch. Design-oriented models are popular for design engineers because of their simplicity and accuracy at the same time. Many of previous studies related the stress-strain curve to the ultimate condition of FRP-confined concrete [24,25,46,48,71,80]. The ultimate condition of FRP-confined concrete is composed of the ultimate confined concrete strength (f'_{cc}) and ultimate confined concrete strain (ε_{cc}). Since many of the studies performed separate statistical regression to find the ultimate concrete strain and strength, there is a possibility that the ultimate strain and stress do not yield on the stress-strain curve of the confined concrete. Thus, the stress-strain curves that are built based on the ultimate condition may predict a different secondary slope that is related to the confinement. In addition, in the prediction of the confined concrete strength and strain, the confining pressure (f_l) is involved as defined in Eq. 24 per ACI 440-2R [44].

$$f_l = \frac{2E_f t_f \varepsilon_{fe}}{D} \; ; \; \varepsilon_{fe} = k_e \varepsilon_{fu} \tag{24}$$

where E_f and t_f are the modulus of elasticity and the thickness of the FRP wrap, respectively, D is the diameter of the concrete member, ε_{fe} is the effective rupture strain, ε_{fu} is the ultimate tensile strain of FRP found from the coupon tests, and k_e is the strain efficiency factor. The strain efficiency factor is considered as 0.55 per ACI 440.2R [44], and as a constant in most of the studies. However, multiple studies are proposing a variable strain efficiency factor [76–78,81–83]. In the current study, the strain efficiency factor was found as 0.7 which is the average of 788 data points. The performance of the strain efficiency factor of 0.7 has also been verified by Sadeghian and Fillmore [84]. The point of using effective rupture stain and its variability inserts lots of uncertainties in the prediction of the confining pressure at the ultimate condition and in turn the prediction of the ultimate condition. Therefore, the use of the confining pressure in the stress-strain curves through the ultimate condition is one of the sources of inaccuracy. The elimination of the rupture strain from the predicting equations for the stress-strain relationships leads to the confinement modulus (E_L) which only relates to the properties of the FRP wrap and the column diameter as shown in Eq. 25.

$$E_L = \frac{2E_f t_f}{D} \; ; \; f_l = E_L \, \varepsilon_{fe} \tag{25}$$

To find the stress-strain curve for the FRP-confined concrete columns, a four-parameter Richard and Abbott model [69] was adopted. The model is presented in the format of a power equation which consists of an initial ascending portion followed by a secondary linear portion up to the ultimate condition, as presented in Fig. 8. The four parameters of the curve are the initial modulus of elasticity (E_1), the secondary modulus of elasticity (E_2), a polynomial constant (n) which to fit a smooth transition between the two portions, and f_o which is the intercept stress

defined as the intersection of the secondary portion and the vertical stress axis. Eq. 26 presents the curve equation which relates the stress (f_c) to the strain (ε_c) for the confined concrete.

$$f_c = \frac{(E_1 - E_2)\varepsilon_c}{\left[1 + \left(\frac{(E_1 - E_2)\varepsilon_c}{f_o}\right)^n\right]^{1/n}} + E_2\varepsilon_c \tag{26}$$

The model was first adjusted by Samaan et al. [21] to predict the stress-strain curve of concrete-filled FRP tubes (CFFTs) and later it was validated for CFRP-wrapped concrete specimens [85]. Since the FRP wraps are mainly activated at a level of lateral expansion in the vicinity of the unconfined concrete strength, the initial slope (E_1) was adopted from ACI 318 [86] equation and the rest of the parameters were calibrated based on 30 tests of confined concrete presented in the study performed by Samaan et al. [21]. The secondary modulus was considered as a function of the stiffness of the confining tubes in the hoop direction, and the unconfined strength of the concrete. Also, the intercept stress was considered as a function of unconfined concrete strength and the confining pressure, and the polynomial constant was chosen as 1.5. Later, Xiao and Wu [70] improved the estimation of the parameters based on an updated database and a new approach. The secondary slope was found when the stress of confined concrete reaches the yield surface which involves the axial and confining pressure relationship and the initial slope of axial-lateral strain curves. The intercept stress was derived as the coefficient of reference plastic strength using regression analysis, and the constant n was selected as 2. In another study, Wu et al. [71] proposed a modification to the proposed parameters by Samaan et al. [21]for high strength concrete columns confined by Aramid FRP (AFRP) and set the constant n equal to 2.5. It should be mentioned that for the secondary slope, instead of the confining stiffness, the ultimate condition for AFRPs was used. Djafar-Henni and Kassoul [73] used a database of 81 AFRP-confined concrete columns and proposed a new estimation of the parameters presented in Eq. 26 for AFRP

confined concrete with a constant n equal to 2.25. Lobo et al. [64] developed a model for AFRPs using 29 specimens, proposed new equations for the curve parameters, and found the constant n as $\sqrt{2}$. Also, Jesus et al. [13] proposed a model for GFRPs using 60 specimens. It should be mentioned that for the last four introduced studies, the secondary slope was a function of the ultimate condition. Later, Bai et al. [14] found the curve parameters for large rupture strain FRP-confined concrete using a database of 62 specimens.

In the current study, a reduced database including 200 full stress-strain curves from sixteen independent studies was extracted from the literature as presented in Table 5. The selected curves included 130 carbon, 22 aramid, 42 glass, and 6 basalt FRP-wrapped concrete columns. This is the broadest database of full stress-strain curves (not the ultimate condition) that have been collected for the calibration of the four parameters of the Richard and Abbott model [69]. To calibrate the parameters, a parabola was fitted to the first portions of the curves and the initial slope of the parabola was considered as the initial modulus of elasticity (E_1). Also, a straight line was fitted to all secondary portions of the curve and the slope of the curves was found as the slope of the fitted line (E_2) and the intercept stress was evaluated as the line intercepts the stress axis (f_o). For each curve, the values of the initial slope, secondary slope, the intercept stress, and the confining stiffness are presented in Table 5. Also, the ratio of the secondary slope to the initial slope (E_2/E_1) and the ratio of the intercept stress to the unconfined concrete strength (f_o/f_{co}) were presented in Table 5. To show the range of the data used in the database, the mean, standard deviation (STD), and the coefficient of variation (COV) of each column are presented at the end of Table 5.

To drive equations for the parameters of the stress-strain curve, a regression analysis was performed by considering the confining stiffness (E_L) and unconfined concrete strength (f'_{co}) as the effective parameters. For the initial slope for the first region, the regression showed the best-

fitted equation as $E_1 = 4691\sqrt{f'_{co}}$ with ($R^2 = 0.4818$) which is quite close to the prediction of unconfined concrete modulus proposed by ACI 318 [86]. Thus, Eq.27 from ACI 318 [86] was adopted instead of the one found from the regression. Eq. 27 through Eq. 29 show the results of the regression analysis, in which all the units are in MPa.

$$E_1 = 4700\sqrt{f'_{co}} \qquad (R^2 = 0.4817) \tag{27}$$

$$E_2 = 9.6\sqrt{E_l}\sqrt{f'_{co}} \qquad (R^2 = 0.8251) \tag{28}$$

$$f_o = (1 + 0.15\frac{\sqrt{E_l}}{f'_{co}})f'_{co} \qquad (R^2 = 0.9083) \tag{29}$$

Eq. 28 predicts the slope of the secondary portion of the stress-strain curves. The equation showed that an increase in confining stiffness and unconfined concrete strength directly increase the secondary modulus of the curve. However, the comparison between the initial slope and the secondary slope shows that the constant coefficient for Eq. 28 is much lower than the one for Eq. 27. The latter is compatible with the results of experimental stress-strain curves presented in Table 5, as the average ratio of secondary to the initial slope of the curve is 7.36 %. The coefficient of determination (R^2) for Eq. 28 is 0.8251 which shows a very good agreement between the experimental results and the prediction as presented in Fig. 9(a).

Eq. 29 predicts the intercept stress as the sum of unconfined concrete strength and a percentage of confining stiffness which is compatible with the results of experimental tests as presented in Table 5. The average ratio of intercept stress to unconfined concrete strength is 1.10 showed in Table 5, which shows an average upward shift of 10% in the intercept stress with respect to the unconfined concrete strength. The additional shift is attributed to the confining stiffness in Eq. 29 which showed a very good agreement with the test results ($R^2 = 0.9083$), as presented in Fig. 9(b). Also, the coefficient of variation of the data is 13% which shows the variability of the

intercept stress, while it was considered as a constant in many of the models. Thus, it is recommended to consider the intercept stress as a variable parameter instead of a constant.

To find the polynomial constant n, all points in 200 curves, which sums to a total of 3272 points (without the origin points), were evaluated by Eq. 26 with parameters introduced in Eq. 27 to Eq. 29, and the polynomial constant n was found to minimize the RMSE error of all points. The results of the analysis showed that a polynomial constant of 2.5 minimizes the error ($n = 2.5$). By substituting curve parameters (Eq. 27 to Eq. 29 and a polynomial constant of 2.5) into Eq. 26, the stress-strain of the FRP-confined concrete can be shown as the following single equation.

$$f_c = 9.6\sqrt{\frac{2E_f t_f f'_{co}}{D}}\left\{1 + \left(489.6\sqrt{\frac{D}{2E_f t_f}} - 1\right)\left[1 + \left(\frac{4700 - 9.6\sqrt{\frac{2E_f t_f}{D}}}{\sqrt{f'_{co}} + 0.15\sqrt{\frac{2E_f t_f}{Df'_{co}}}}\varepsilon_c\right)^{2.5}\right]^{-1/2.5}\right\}\varepsilon_c \tag{30}$$

To evaluate the performance of the proposed model, fourteen design-oriented stress-strain curves for FRP-confined concrete columns were compared with the experimental curves, as presented in Table 6. In addition to RMSE and AAE (Eqs.19 and 20), two more measures of error were considered (Eqs.31 and 32) for mean square error (MSE) and standard deviation (SD).

$$MSE = \frac{\sum\left(\frac{Calc._i - Exp._i}{Exp._i}\right)^2}{N} \tag{31}$$

$$SD = \sqrt{\frac{\sum\left(\frac{Calc._i}{Exp._i} - \frac{Calc._{ave}}{Exp._{ave}}\right)^2}{N - 1}} \tag{32}$$

Table 6 shows that the proposed stress-strain curve improved the available design-oriented confined stress-strain curves. The distribution of the error measures for the current study and the curve proposed by Lam and Teng [25], which is the base for the ACI 440.2R [44], is presented in

Fig. 10. The comparison of the error distribution showed that the model improved the error of every curve considerably, in addition to the overall error presented in Table 6.

Some samples of the fitted curves are presented in Fig. 11 which compares the experimental curves from different studies with the five of the best estimations of the stress-strain curves according to Table 6. The results showed the proposed stress-strain curves are in very good agreement with the experimental test results. It should be mentioned that in the formulas showed in Fig. 11, rather than the proposed equation in this study, the intercept stress was considered constant. Also, for equations proposed by Lam and Teng [25] and Teng et al. [24], the secondary is related to the ultimate condition. The results showed that for some cases, using these equations for the prediction leads to a very good fit [as shown in Fig. 11(f), (h), (i), (j), and (k)]. However, for some cases, the slope would not be matched with the experimental results [as shown in Fig. 11(b), (c), (e), and (g)], and for some cases, although the slope is matched, the constant stress intercept leads to lowering down the curves [as shown in Fig. 11(a), (d), and (l)]. For the proposed model in this study, the intercept stress is a variable that shifts the secondary part up and down, and the ultimate condition is only a point on the curve that cuts the curve and does not affect the secondary slope. Also, the curve predictions by Fahmy and Wu [63] showed better predictions in comparison to proposed curves by Lam and Teng [25] and Teng et al. [24], since the secondary slope was selected independent of the ultimate condition although the main equation format kept the same as Lam and Teng [25]. Thus, it can be concluded that excluding the ultimate condition from the adjustment of stress-strain curves of confined concrete lead to more accurate predictions. Then, the ultimate condition can be used as a cut-off point for the stress-strain curves instead of involving in predicting the curve parameters. It should be mentioned that a safety strain limit of 0.01 mm/mm is considered by ACI 440.2R [44] which is the cutting point of the stress-strain

curves for most situations. In the main database including 788 tests, the minimum axial strain at the time of FRP rupture was 0.019 mm/mm. The latter shows that the ultimate condition does not enter the analysis which leads to the designs, as a cutting point of 0.01 mm/mm occur prior to the ultimate confined strain for the majority of cases and govern the designs, although the ultimate confined strain is very effective for analysis purposes which tends to assess the most accurate behavior of the structures without design limitations.

5. COMPARISON OF THE ULTIMATE STRAIN EQUATIONS

In this study, the ultimate confined strain is defined as the axial strain corresponding to the ultimate confined concrete strength on the stress-strain curve as presented in Eq. 35.

$$\varepsilon_{cc} = \frac{f'_{cc} - f_o}{E_2} \tag{33}$$

Since Eq. 33 is not directly found from the regression analysis on the ultimate strains available in the database, the ultimate strain and stress kept their correlation. It should be highlighted that the rupture strain affects directly the prediction of ultimate stress and strain through the confining pressure. This study suggests the use of a strain efficiency of 0.7 which is the average ratio of the rupture strain of FRP wrap in the hoop direction to the ultimate tensile strength of FRP coupons available in the database.

To examine the fineness of the proposed ultimate strain equation, the predictions from four selected studies were compared [24,87–89]. In 2009, Teng et al. [24] refined the design-oriented stress-strain model for FRP-confined concrete proposed by Lam and Teng [25] based on experimental tests and an accurate analysis-oriented stress-strain model and regression. Table 7 presents the proposed estimation for the ultimate confined strain defined by Teng et al. [24].

In 2013, Pham and Hadi [87] estimated the ultimate for CFRP-confined concrete columns using an energy approach. The concept was introduced by Mander et al. [13] which stated that the additional energy absorption in the concrete core is the same as the total work done by the FRP wrap. However, it was realized by Pham and Hadi [87] that the volumetric strain energy of FRP was proportional to the volumetric strain energy of the confined concrete by a factor k. The ultimate confined strain and the proportional factor k were found for a database including 98 circular columns and 69 square specimens via regression analysis, as presented in Table 7.

In 2015, Lim and Ozbakkaloglu [88] proposed a model that predicts the dilation characteristic of the FRP-confined concrete for passively and actively confined concrete based on regression analysis on a large database. It should be noted that the strain efficiency factor (k_e) was found as a function of the unconfined concrete strength and the modulus of elasticity of the FRP wrap in the hoop direction. Table 7 presented the ultimate confined strain from the axial-lateral relationship evaluated at the rupture strain, provided by Lim and Ozbakkaloglu [88].

In 2017, Wu and Cao [89] improved the strain model using the energy balance method and regression analysis. Inside the model, a strain efficiency factor of 0.9 ($k_e = 0.9$) was used. While Hadi and Pham [87] defined a constant value for the proportional factor k (introduced earlier), Wu and Cao [88] proposed a parametric equation for this factor as presented in Table 7.

Using Eqs.30 and 33, the ultimate confined strain for all the data points was evaluated as the proposed prediction, as presented in Table 7. Also, Table 7 shows the fineness of the model by comparing the prediction versus experimental values for the models adjusted in the current study and some of the models available in the literature by RMSE and AAE error measures. The model was evaluated using the actual hoop rupture strain to compare to the models developed by Teng et al. [24] and Pham and Hadi [87]. However, the model was evaluated using a strain efficiency factor

of 0.7 to be compared with the models developed by Lim and Ozbakkaloglu [88] and Wu and Cao [89] as they developed their models based on different strain efficiency factors. The results showed that the proposed model is rational and improved the compared models for ultimate confined strain by comparing RMSE error for the database. It should be mentioned that the model proposed by Lim and Ozbakkaloglu [88] showed a better AAE error, which proposed a variable strain efficiency factor, in comparison with the model adjusted in this study, in which a constant strain efficiency factor of 0.7 was used. Overall, the prediction of the ultimate confined strain using the proposed model showed a very good agreement with the experimental results.

6. CONCLUSION

In this paper, a five-parameter Willam-Warnke failure criterion was used to develop an equation for ultimate confined strength using 788 datapoints. The model improved the available plasticity-based models and showed a very good agreement with the experimental tests. In addition, a design-oriented model for the stress-strain curve of FRP-wrapped concrete columns was calibrated using 200 full stress-strain curves from sixteen different sets of experimental tests which extracted an overall 3272 different points from the literature by adopting a general expression of Richard and Abbott. The initial slope, secondary slope, and intercept stress for all the curves were found and reported in the paper. The stress-strain curve and ultimate strength were utilized to obtain the ultimate strain condition without direct regression analysis of the database. The following conclusions can be drawn:

- The proposed stress-strain curve (Eq. 30) is related only to the unconfined concrete strength, modulus of elasticity and thickness of FRP wrap, and the diameter of the column.
- Excluding the ultimate condition from the adjustment of stress-strain curves of confined concrete leads to more accurate predictions, as it eliminates the effect of rupture strain

which imposes a large variability in the predictions. The ultimate condition was recognized only as the cut-off point for the stress-strain curve. Also, the intercept stress was considered as a variable improving the slope and location of the secondary portion of the curve.

- The proposed stress-strain curve was in very good agreement with the experimental test results and the prediction improved the available predictions in the literature by showing the least error in comparison to fourteen different studies.

- The study of 200 stress-strain curves of FRP-confined columns revealed an average and standard deviation of 1.10 and 13 % for the ratio of the intercept stress to the unconfined concrete strength, respectively. The latter shows the variability of the intercept stress while it was considered as a constant value in many of the available models. Therefore, considering the intercept stress as a variable is suggested instead of a constant value.

- The ultimate confined strain was derived using the stress-strain curve and the ultimate confined strength which kept the correlation of the ultimate confined strength, ultimate confined strain, and the confining pressure by making them interrelated. A comparison of the ultimate confined strain prediction showed that the predicted values are in very good agreement with the experimental tests.

- A comparison of the developed model for the ultimate strength in this study and the model proposed by ACI 440.2R showed that the model is not conservative for normalized confining pressure to unconfined concrete strength ratio of less than 0.2 or more than 1. However, more data are required to assess the need to be more conservative for confining pressures of more than 1. Also, a new normalized confining pressure of 0.05 was introduced as the confining limit after which the FRP-confined concrete can be activated.

- The findings of this study are applicable in the range of examined databases, as presented in Table 1. Also, the study does not cover stress-strain curves with a secondary descending branch due to lack of confinement.

7. ACKNOWLEDGEMENTS

8. DATA AVAILABILITY STATEMENT

Some or all data, models, or code generated or used during the study are available from the corresponding author by request (including test data).

9. REFERENCES

[1]   Jawdhari A, Adheem AH, Kadhim MMA. Parametric 3D finite element analysis of FRCM-confined RC columns under eccentric loading. Engineering Structures 2020; 212:110504. https://doi.org/10.1016/j.engstruct.2020.110504.

[2]   Piscesa B, Attard MM, Samani AK. 3D Finite element modeling of circular reinforced concrete columns confined with FRP using a plasticity based formulation. Composite Structures 2018; 194:478–93. https://doi.org/10.1016/j.compstruct.2018.04.039.

[3]   Ferrotto MF, Fischer O, Cavaleri L. A strategy for the finite element modeling of FRP-confined concrete columns subjected to preload. Engineering Structures 2018; 173:1054–67. https://doi.org/10.1016/j.engstruct.2018.07.047.

[4]   Yu T, Teng JG, Wong YL, Dong SL. Finite element modeling of confined concrete-I: Drucker-Prager type plasticity model. Engineering Structures 2010; 32:665–79. https://doi.org/10.1016/j.engstruct.2009.11.014.

[5]   Moran DA, Pantelides CP, Reaveley LD. Mohr-coulomb model for rectangular and square FRP-confined concrete. Composite Structures 2019; 209:889–904. https://doi.org/10.1016/j.compstruct.2018.11.024.

[6]   Moran DA, Pantelides CP. Elliptical and circular FRP-confined concrete sections: A Mohr-Coulomb analytical model. International Journal of Solids and Structures 2012; 49:881–98. https://doi.org/10.1016/j.ijsolstr.2011.12.012.

[7]   Jiang JF, Wu YF. Characterization of Yield Surfaces for FRP-Confined Concrete. Journal of Engineering Mechanics 2014;140. https://doi.org/10.1061/(ASCE)EM.1943-7889.0000811.

[8]   Jiang JF, Wu YF. Plasticity-based criterion for confinement design of FRP jacketed concrete columns. Materials and Structures/Materiaux et Constructions 2016; 49:2035–51. https://doi.org/10.1617/s11527-015-0632-4.

[9]   Mohammadi M, Dai JG, Wu YF, Bai YL. Development of extended Drucker–Prager model for non-uniform FRP-confined concrete based on triaxial tests. Construction and Building Materials 2019; 224:1–18. https://doi.org/10.1016/j.conbuildmat.2019.07.061.

[10]   Ozbakkaloglu T, Gholampour A, Lim JC. Damage-Plasticity Model for FRP-Confined Normal-Strength and High-Strength Concrete. Journal of Composites for Construction 2016; 20:1–13. https://doi.org/10.1061/(ASCE)CC.1943-5614.0000712.

[11]   Mohammadi M, Wu YF. Modified plastic-damage model for passively confined concrete based on triaxial tests. Composites Part B: Engineering 2019; 159:211–23. https://doi.org/10.1016/j.compositesb.2018.09.074.

[12]   Saberi H, Bui TQ, Furukawa A, Rahai A, Hirose S. FRP-confined concrete model based

on damage-plasticity and phase-field approaches. Composite Structures 2020;244.

https://doi.org/10.1016/j.compstruct.2020.112263.

[13]   Mander JB, Priestley MJN, Park R. Theoretical Stress-Strain Model for Confined

Concrete. Journal of Structural Engineering 1988; 114:1804–26.

https://doi.org/10.1061/(ASCE)0733-9445(1988)114:8(1804).

[14]   Bing L, Park R, Tanaka H. Stress-strain behavior of high-strength concrete confined by

ultra-high- and normal-strength transverse reinforcements. ACI Structural Journal 2001;

98:395–406. https://doi.org/10.14359/10228.

[15]   Afifi MZ, Mohamed HM, Benmokrane B. Theoretical stress-strain model for circular

concrete columns confined by GFRP spirals and hoops. Engineering Structures 2015;

102:202–13. https://doi.org/10.1016/j.engstruct.2015.08.020.

[16]   Hales TA, Pantelides CP, Sankholkar P, Reaveley LD. Analysis-oriented stress-strain

model for concrete confined with fiber-reinforced polymer spirals. ACI Structural Journal

2017; 114:1263–72. https://doi.org/10.14359/51689788.

[17]   Wu Y-F, Zhou Y-W. Unified Strength Model Based on Hoek-Brown Failure Criterion

for Circular and Square Concrete Columns Confined by FRP. Journal of Composites for

Construction 2010; 14:175–84. https://doi.org/10.1061/(ASCE)CC.1943-5614.0000062.

[18]   Yan Z, Pantelides CP, Reaveley LD. Fiber-reinforced polymer jacketed and shape-

modified compression members: I - Experimental behavior. ACI Structural Journal 2006;

103:885–93.

[19]   Karbhari VM, Gao Y. Composite Jacketed Concrete under Uniaxial Compression—Verification of Simple Design Equations. Journal of Materials in Civil Engineering 1997; 9:185–93. https://doi.org/10.1061/(ASCE)0899-1561(1997)9:4(185).

[20]   Richart FE, Brandtzaeg A, Brown RL. A study of the failure of concrete under combined compressive stresses. In: Bulletin No 185, Univ of Illinois, Eng. Experimental Station: Champaign, Ill 1928.

[21]   Samaan M, Mirmiran A, Shahawy M. Model of concrete confined by fiber composites. Journal of Structural Engineering 1998; 124:1025–31. https://doi.org/10.1061/(ASCE)0733-9445(1998)124:9(1025).

[22]   Saafi M, Toutanji HA, Li Z. Behavior of concrete columns confined with fiber reinforced polymer tubes. ACI Materials Journal 1999; 96:500–9. https://doi.org/10.14359/652.

[23]   Mirmiran A., Shahawy M. Behavior of concrete columns confined by fiber composites, Journal of Structural Engineering 1997, 123(5):583-590.

[24]   Teng JG, Jiang T, Lam L, Luo YZ. Refinement of a design-oriented stress–strain model for FRP-confined concrete. Journal of Composites for Construction 2009; 13:269–78. https://doi.org/10.1061/(ASCE)CC.1943-5614.0000012.

[25]   Lam L, Teng JG. Design-oriented stress-strain model for FRP-confined concrete. Construction and Building Materials, 2003; 17:471–89. https://doi.org/10.1016/S0950-0618(03)00045-X.

[26]   Sadeghian P, Fam A. Improved design-oriented confinement models for FRP-wrapped concrete cylinders based on statistical analyses. Engineering Structures 2015; 87:162–82. https://doi.org/10.1016/j.engstruct.2015.01.024.

[27]   Fallah Pour A, Ozbakkaloglu T, Vincent T. Simplified design-oriented axial stress-strain model for FRP-confined normal- and high-strength concrete. Engineering Structures 2018; 175:501–16. https://doi.org/10.1016/j.engstruct.2018.07.099.

[28]   Bisby LA, Dent AJS, Green MF. Comparison of confinement models for fiber-reinforced polymer-wrapped concrete. ACI Structural Journal 2005; 102:62–72. https://doi.org/10.14359/13531.

[29]   Willam JK, Warnke EP. Constitutive model for the triaxial behaviour of concrete. Proc Intl Assoc Bridge Structural Engineers 1975; 19:1–30.

[30]   Khorramian K. Short and Slender Concrete Columns Internally or Externally Reinforced with Longitudinal Fiber-Reinforced Polymer Composites . PhD Thesis, Dalhousie University, Halifax, NS, Canada, 2020.

[31]   Jiang K, Han Q, Bai Y, Du X. Data-driven ultimate conditions prediction and stress-strain model for FRP-confined concrete. Composite Structures 2020; 242:112094. https://doi.org/10.1016/j.compstruct.2020.112094.

[32]   Naderpour H, Mirrashid M. Advances in civil engineering materials confinement coefficient predictive modeling of FRP-confined RC columns 2020. https://doi.org/10.1520/ACEM20190145.

[33]   Ceccato C, Teng JG, Cusatis G. Numerical prediction of the ultimate condition of circular concrete columns confined with a fiber reinforced polymer jacket. Composite Structures 2020; 241:112103. https://doi.org/10.1016/j.compstruct.2020.112103.

[34]   Li P, Wu YF, Zhou Y, Xing F. Stress-strain model for FRP-confined concrete subject to arbitrary load path. Composites Part B: Engineering 2019; 163:9–25. https://doi.org/10.1016/j.compositesb.2018.11.002.

[35]   Spoelstra MR, Monti G. FRP-confined concrete model. Journal of Composites for Construction 1999; 3:143–50. https://doi.org/10.1061/(ASCE)1090-0268(1999)3:3(143).

[36]   Fam AZ, Rizkalla SH. Confinement model for axially loaded concrete confined by circular fiber-reinforced polymer tubes. ACI Structural Journal 2001; 98:451–61. https://doi.org/10.14359/10288.

[37]   Jiang T, Teng JG. Analysis-oriented stress-strain models for FRP-confined concrete. Engineering Structures 2007; 29:2968–86. https://doi.org/10.1016/j.engstruct.2007.01.010.

[38]   Xiao QG, Teng JG, Yu T. Behavior and modeling of confined high-strength concrete. Journal of Composites for Construction 2010; 14:249–59. https://doi.org/10.1061/(ASCE)CC.1943-5614.0000070.

[39]   Moran DA, Pantelides CP. Stress-strain model for fiber-reinforced polymer-confined concrete. Journal of Composites for Construction 2002; 6:233–40. https://doi.org/10.1061/(ASCE)1090-0268(2002)6:4(233).

[40]   Binici B. An analytical model for stress-strain behavior of confined concrete. Engineering Structures 2005; 27:1040–51. https://doi.org/10.1016/j.engstruct.2005.03.002.

[41]   Pan Y, Guo R, Li H, Tang H, Huang J. Analysis-oriented stress–strain model for FRP-confined concrete with preload. Composite Structures 2017; 166:57–67. https://doi.org/10.1016/j.compstruct.2017.01.007.

[42]   Yang J, Wang J, Wang Z. Axial compressive behavior of partially CFRP confined seawater sea-sand concrete in circular columns – Part II: A new analysis-oriented model.

Composite Structures 2020; 246:112368.

https://doi.org/10.1016/j.compstruct.2020.112368.

[43]   Ferrotto MF, Fischer O, Cavaleri L. Analysis-oriented stress–strain model of CFRP-
        confined circular concrete columns with applied preload. Materials and Structures 2018;
        51:1–16. https://doi.org/10.1617/s11527-018-1169-0.

[44]   ACI (American Concrete Institute). Guide for the design and construction of externally
        bonded FRP systems for strengthening concrete structures. Farmington Hills, MI: ACI
        440.2R-17; 2017.

[45]   CSA (Canadian Standards Association). Design and construction of building structures
        with fibre-reinforced polymers. Mississauga, ON: CAN / CSA S806-12; 2012.

[46]   Fardis MN, Khalili HH. FRP-encased concrete as a structural material. Magazine of
        Concrete Research 1982; 34:191–202. https://doi.org/10.1680/macr.1982.34.121.191.

[47]   Ahmad SH, Khaloo AR, Irshaid A. Behaviour of concrete spirally confined by fibreglass
        filaments. Magazine of Concrete Research 1991; 43:143–8.
        https://doi.org/10.1680/macr.1991.43.156.143.

[48]   Saadatmanesh H, Ehsani MR, Li MW. Strength and ductility of concrete columns
        externally reinforced with fiber composite straps. Structural Journal. 1994; 91:434-47.

[49]   Li YF, Lin CT, Sung YY. A constitutive model for concrete confined with carbon fiber
        reinforced plastics. Mechanics of Materials, 2003; 35:603–19.
        https://doi.org/10.1016/S0167-6636(02)00288-0.

[50]   Popovics S. A numerical approach to the complete stress-strain curve of concrete.
        Cement and Concrete Research 1973; 3:583–99. https://doi.org/10.1016/0008-
        8846(73)90096-3.

[51]   Demers M, Neale KW. Strengthening of concrete columns with unidirectional composite sheets. Developments in short and medium span bridge engineering. 1994; 895-905.

[52]   Karbhari VM, Gao Y. Composite jacketed concrete under uniaxial compression—verification of simple design equations. Journal of Materials in Civil Engineering 1997; 9:185–93. https://doi.org/10.1061/(ASCE)0899-1561(1997)9:4(185).

[53]   Xiao Y, Wu H. Compressive behavior of concrete confined by carbon fiber composite jackets. Journal of Materials in Civil Engineering 2000; 12:139–46. https://doi.org/10.1061/(ASCE)0899-1561(2000)12:2(139).

[54]   Saiid Saiidi M, Sureshkumar K, Pulido C. Simple carbon-fiber-reinforced-plastic-confined concrete model for moment-curvature analysis. Journal of Composites for Construction 2005; 9:101–4. https://doi.org/10.1061/(ASCE)1090-0268(2005)9:1(101).

[55]   Binici B. Design of FRPs in circular bridge column retrofits for ductility enhancement. Engineering Structures 2008; 30:766–76. https://doi.org/10.1016/j.engstruct.2007.05.012.

[56]   Hognestad E. A study of combined bending and axial load in reinforced concrete members. Bulletin Series No 399 1951:128. https://doi.org/10.14359/7785.

[57]   Miyauchi K, Nishibayashi S, Inoue S. Estimation of Strengthening Effects with Carbon Fiber Sheet for Concrete Column. In: Proceedings of the Third International Symposium on Non-Metallic FRP for Concrete Structures, 1997; 224.

[58]   Jolly CK, Lilistone D. The stress–strain behavior of concrete confined by advanced fibre composites. In: Proc. 8th BCA conference higher education and the concrete industry. Southampton 1998.

[59]   Miyauchi K, Inoue S, Kuroda T, Kobayashi A. Strengthening effects with carbon fiber sheet for concrete column. Proc Jpn Concr Inst 1999; 21:1453-8.

[60]   Lillistone D, Jolly CK. An innovative form of reinforcement for concrete columns using advanced composites. Structural Engineer 2000; 78:20–8.

[61]   Jiang T, Teng J. Strengthening of short circular RC columns with FRP jackets: a design proposal 2006.

[62]   Yu T, Teng JG. Design of concrete-filled FRP tubular columns: provisions in the Chinese technical code for infrastructure application of FRP composites. Journal of Composites for Construction 2011; 15:451–61. https://doi.org/10.1061/(ASCE)CC.1943-5614.0000159.

[63]   Fahmy MFM, Wu Z. Evaluating and proposing models of circular concrete columns confined with different FRP composites. Composites Part B: Engineering 2010; 41:199–213. https://doi.org/10.1016/j.compositesb.2009.12.001.

[64]   Bai YL, Dai JG, Mohammadi M, Lin G, Mei SJ. Stiffness-based design-oriented compressive stress-strain model for large-rupture-strain (LRS) FRP-confined concrete. Composite Structures 2019; 223:110953. https://doi.org/10.1016/j.compstruct.2019.110953.

[65]   Toutanji HA. Stress-strain characteristics of concrete columns externally confined with advanced fiber composite sheets. ACI Materials Journal 1999; 96:397–404. https://doi.org/10.14359/639.

[66]   Sargin M. Stress-strain relationships for concrete and analysis of structural concrete sections. Study No 4, Solid Mechanics Division, University of Waterloo, Waterloo, Ontario, Canada 1971.

[67]   Ahmad SH, Shah SP. Complete triaxial stress-strain curves for concrete. ASCE J Struct Div 1982; 108:728–42.

[68]   Berthet JF, Ferrier E, Hamelin P. Compressive behavior of concrete externally confined by composite jackets: Part B: Modeling. Construction and Building Materials 2006; 20:338–47. https://doi.org/10.1016/j.conbuildmat.2005.01.029.

[69]   R. M. Richard, B. J. Abbott. Versatile elastic-plastic stress-strain formula. Journal of the Engineering Mechanics Division 1975; 101:511–5.

[70]   Xiao Y, Wu H. Compressive behavior of concrete confined by various types of FRP composite jackets. Journal of Reinforced Plastics and Composites 2003; 22:1187–201. https://doi.org/10.1177/0731684403035430.

[71]   Wu H-L, Wang Y-F, Yu L, Li X-R. Experimental and computational studies on high-strength concrete circular columns confined by aramid fiber-reinforced polymer sheets. Journal of Composites for Construction 2009; 13:125–34. https://doi.org/10.1061/(ASCE)1090-0268(2009)13:2(125).

[72]   Wu HL, Wang YF. Experimental study on reinforced high-strength concrete short columns confined with AFRP sheets. Steel and Composite Structures 2010; 10:501–16. https://doi.org/10.12989/scs.2010.10.6.501.

[73]   Djafar-Henni I, Kassoul A. Stress–strain model of confined concrete with Aramid FRP wraps. Construction and Building Materials 2018; 186:1016–30. https://doi.org/10.1016/j.conbuildmat.2018.08.013.

[74]   Jesus M, Silva Lobo P, Faustino P. Design models for circular and square RC columns confined with GFRP sheets under axial compression. Composites Part B: Engineering 2018; 141:60–9. https://doi.org/10.1016/j.compositesb.2017.12.043.

[75]   Silva Lobo P, Faustino P, Jesus M, Marreiros R. Design model of concrete for circular columns confined with AFRP. Composite Structures 2018; 200:69–78. https://doi.org/10.1016/j.compstruct.2018.05.094.

[76]   Sadeghian P, Fam A. A rational approach toward strain efficiency factor of fiber-reinforced polymer-wrapped concrete columns. ACI Structural Journal 2014; 111:135–44. https://doi.org/10.14359/51686437.

[77]   Sadeghian P, Seracino R, Das B, Lucier G. Influence of geometry and fiber properties on rupture strain of cylindrical FRP jackets under internal ICE pressure. Composite Structures 2018; 192:173–83. https://doi.org/10.1016/j.compstruct.2018.02.077.

[78]   Chen JF, Li SQ, Bisby LA. Factors affecting the ultimate condition of FRP-wrapped concrete columns. Journal of Composites for Construction 2013; 17:67–78. https://doi.org/10.1061/(ASCE)CC.1943-5614.0000314.

[79]   Chen W-F. Plasticity in reinforced concrete. McGraw-Hill; 1982.

[80]   Samaan M, Mirmiran A, Shahawy M. Model of concrete confined by fiber composites. Journal of Structural Engineering 1998; 124:1025–31. https://doi.org/10.1061/(ASCE)0733-9445(1998)124:9(1025).

[81]   Wu YF, Jiang JF. Effective strain of FRP for confined circular concrete columns. Composite Structures 2013; 95:479–91. https://doi.org/10.1016/j.compstruct.2012.08.021.

[82]   El-Hacha R, Abdelrahman K. Slenderness effect of circular concrete specimens confined with SFRP sheets. Composites Part B: Engineering 2013; 44:152–66. https://doi.org/10.1016/j.compositesb.2012.06.014.

[83]   Smith ST, Kim SJ, Zhang H. Behavior and effectiveness of FRP wrap in the

         confinement of large concrete cylinders. Journal of Composites for Construction 2010;

         14:573–82. https://doi.org/10.1061/(ASCE)CC.1943-5614.0000119.

[84]   Sadeghian P, Fillmore B. Strain distribution of basalt FRP-wrapped concrete cylinders.

         Case Studies in Construction Materials 2018; 9.

         https://doi.org/10.1016/j.cscm.2018.e00171.

[85]   Shahawy M, Mirmiran A, Beitelman T. Tests and modeling of carbon-wrapped concrete

         columns. Composites Part B: Engineering 2000; 31:471–80.

         https://doi.org/10.1016/S1359-8368(00)00021-4.

[86]   ACI (American Concrete Institute). Building code requirements for structural concrete.

         Farmington Hills, Michigan: ACI 318-19; 2019.

[87]   Pham TM, Hadi MNS. Strain estimation of CFRP-confined concrete columns using

         energy approach. Journal of Composites for Construction 2013; 17:1–11.

         https://doi.org/10.1061/(ASCE)CC.1943-5614.0000397.

[88]   Lim JC, Ozbakkaloglu T. Lateral strain-to-axial strain relationship of confined concrete.

         Journal of Structural Engineering (United States) 2015; 141:1–18.

         https://doi.org/10.1061/(ASCE)ST.1943-541X.0001094.

[89]   Wu YF, Cao Y. Energy balance method for modeling ultimate strain of confined

         concrete. ACI Materials Journal 2017; 114:373–81. https://doi.org/10.14359/51689429.

[90]   Teng JG, Jiang T, Lam L, Luo YZ. Refinement of a Design-Oriented Stress – Strain

         Model for FRP-Confined Concrete 2009; 13:269–78.

[91]   Rousakis TC, Rakitzis TD, Karabinis AI. Design-Oriented Strength Model for FRP-Confined Concrete Members. Journal of Composites for Construction 2012; 16:615–25. https://doi.org/10.1061/(ASCE)CC.1943-5614.0000295.

[92]   Fallah Pour A, Ozbakkaloglu T, Vincent T. Simplified design-oriented axial stress-strain model for FRP-confined normal- and high-strength concrete. Engineering Structures 2018; 175:501–16. https://doi.org/10.1016/j.engstruct.2018.07.099.

[93]   Lam L, Teng JG. Ultimate condition of fiber reinforced polymer-confined concrete. Journal of Composites for Construction 2004; 8:539–48. https://doi.org/10.1061/(ASCE)1090-0268(2004)8:6(539).

[94]   Rousakis T, Tepfers R. Behavior of concrete confined by high E-modulus carbon FRP sheets, subjected to monotonic and cyclic axial compressive load. Nordic concrete research-publications 2004; 31:73.

[95]   Berthet JF, Ferrier E, Hamelin P. Compressive behavior of concrete externally confined by composite jackets. Part A: Experimental study. Construction and Building Materials 2005; 19:223–32. https://doi.org/10.1016/j.conbuildmat.2004.05.012.

[96]   Lam L, Teng JG, Cheung CH, Xiao Y. FRP-confined concrete under axial cyclic compression. Cement and Concrete Composites 2006; 28:949–58. https://doi.org/10.1016/j.cemconcomp.2006.07.007.

[97]   Almusallam TH. Behavior of normal and high-strength concrete cylinders confined with E-glass/epoxy composite laminates. Composites Part B: Engineering 2007; 38:629–39. https://doi.org/10.1016/j.compositesb.2006.06.021.

[98]   Wang LM, Wu YF. Effect of corner radius on the performance of CFRP-confined square concrete columns: Test. Engineering Structures 2008;30:493–505. https://doi.org/10.1016/j.engstruct.2007.04.016.

[99]   Benzaid R, Mesbah H, Nasr Eddine Chikh. FRP-confined concrete cylinders: Axial compression experiments and strength model. Journal of Reinforced Plastics and Composites 2010;29:2469–88. https://doi.org/10.1177/0731684409355199.

[100]   Cui C, Sheikh SA. Experimental study of normal- and high-strength concrete confined with fiber-reinforced polymers. Journal of Composites for Construction 2010;14:553–61. https://doi.org/10.1061/(ASCE)CC.1943-5614.0000116.

[101]   Dai JG, Bai YL, Teng JG. Behavior and modeling of concrete confined with FRP composites of large deformability. Journal of Composites for Construction 2011;15:963–73. https://doi.org/10.1061/(ASCE)CC.1943-5614.0000230.

[102]   Wang Z, Wang D, Smith ST, Lu D. Experimental testing and analytical modeling of CFRP-confined large circular RC columns subjected to cyclic axial compression. Engineering Structures 2012;40:64–74. https://doi.org/10.1016/j.engstruct.2012.01.004.

[103]   Lim JC, Ozbakkaloglu T. Hoop strains in FRP-confined concrete columns: experimental observations. Materials and Structures/Materiaux et Constructions 2014;48:2839–54. https://doi.org/10.1617/s11527-014-0358-8.

[104]   Lim JC, Ozbakkaloglu T. Influence of silica fume on stress-strain behavior of FRP-confined HSC. Construction and Building Materials 2014;63:11–24. https://doi.org/10.1016/j.conbuildmat.2014.03.044.

[105]   Lim JC. Axial compressive behavior of actively confined and FRP-confined concretes PhD Dissertation 2015.

[106]   Saadatmanesh H, Ehsani MR, Li MW. Strength and ductility of concrete columns externally reinforced with fiber composite straps. ACI Structural Journal 1994;91:434–47. https://doi.org/10.14359/4151.

[107]   Youssef MN, Feng MQ, Mosallam AS. Stress-strain model for concrete confined by FRP composites. Composites Part B: Engineering 2007;38:614–28. https://doi.org/10.1016/j.compositesb.2006.07.020.

[108]   Ho JC, Ou XL, Chen MT, Wang Q, Lai MH. A path dependent constitutive model for CFFT column. Engineering Structures. 2020;210:110367. https://doi.org/10.1016/j.engstruct.2020.110367.

[109]   Lai MH, Liang YW, Wang Q, Ren FM, Chen MT, Ho JC. A stress-path dependent stress-strain model for FRP-confined concrete. Engineering Structures. 2020;203:109824. https://doi.org/10.1016/j.engstruct.2019.109824.

[110]   Lai MH, Song W, Ou XL, Chen MT, Wang Q, Ho JC. A path dependent stress-strain model for concrete-filled-steel-tube column. Engineering Structures. 2020;211:110312. https://doi.org/10.1016/j.engstruct.2020.110312.

[111]   Dong CX, Kwan AK, Ho JC. A constitutive model for predicting the lateral strain of confined concrete. Engineering Structures. 2015;91:155-66. https://doi.org/10.1016/j.engstruct.2015.02.014.

[112]   Kwan AK, Dong CX, Ho JC. Axial and lateral stress–strain model for FRP confined concrete. Engineering Structures. 2015;99:285-95. https://doi.org/10.1016/j.engstruct.2015.04.046.

Table. 1. Summary of the experimental database for FRP-wrapped concrete specimens.

Material	No.	Parameter	Unit	Mean	STD	COV (%)	Min.	Max.
Concrete	1	D_c	mm	154.00	47.13	31	51.00	406.00
	2	f'_{co}	MPa	52.1	29.4	57	16.6	188.2
FRP Wrap	3	t_f	mm	0.83	0.91	111	0.09	7.26
	4	E_f	GPa	178.53	117.66	66	10.50	662.50
	5	f_f	MPa	2710.1	1337.8	49	220.0	4441.0
	6	ε_f	mm/mm	0.01785	0.00698	39	0.00255	0.04690

Note: STD = standard deviation; COV = coefficient of variation; Min. = minimum; Max. = maximum; D_c = diameter of concrete specimen; f'_{co} = unconfined concrete strength; t_f = thickness of FRP wrap; E_f = modulus of elasticity of FRP wrap; and f_f = tensile strength of FRP wrap.

Table 2. Comparison of some of the plasticity-based formulas in octahedral space.

Model	Year	Compressive meridian equation	RMSE	AAE
Current study (Eq. 11)	2020	$\bar{\tau}_{oct} = 0.1546 - 0.8293\bar{\sigma}_{oct} - 0.0750\bar{\sigma}_{oct}^2$	0.0993	0.0785
Yan et al. [18] [*]	2006	$\bar{\tau}_{oct} = 0.0546 - 1.0218\bar{\sigma}_{oct} - 0.1362\bar{\sigma}_{oct}^2$	0.1402	0.0991
Mander et al. [13]	1988	$\bar{\tau}_{oct} = 0.1230 - 1.1505\bar{\sigma}_{oct} - 0.3155\bar{\sigma}_{oct}^2$	0.1949	0.1301
Hales et al. [16] [*]	2017	$\bar{\tau}_{oct} = 0.2684 - 0.7129\bar{\sigma}_{oct} - 0.3119\bar{\sigma}_{oct}^2$	0.3956	0.2029
Bing et al. [14]	2001	$\bar{\tau}_{oct} = 0.113 - 1.26\bar{\sigma}_{oct} - 0.559\bar{\sigma}_{oct}^2$	0.4363	0.1587
Afifi et al. [15]	2015	$\bar{\tau}_{oct} = -0.1229 - 2.541\bar{\sigma}_{oct} - 1.98\bar{\sigma}_{oct}^2$	1.6977	0.5024

Note: * the presented coefficients are derived based on Eq.16 to 18.

Table 3. Comparison of plasticity-based models.

Model	Year	Formula	RMSE	AAE
Current study (Eq. 15)	2020	$\dfrac{f'_{cc}}{f'_{co}} = -11.702 + 12.702\sqrt{1 + 0.935\dfrac{f_l}{f'_{co}} - 2\dfrac{f_l}{f'_{co}}}$	0.3647	0.1335
Current study (Eq. 14)	2020	$\dfrac{f'_{cc}}{f'_{co}} = -11.702 + 12.470\sqrt{1 + 1.092\dfrac{f_l}{f'_{co}} - 2\dfrac{f_l}{f'_{co}}}$	0.3791	0.1324
Yan et al. [18]	2006	$\dfrac{f'_{cc}}{f'_{co}} = -4.322 + 4.721\sqrt{1 + 4.193\dfrac{f_l}{f'_{co}} - 2\dfrac{f_l}{f'_{co}}}$	0.4269	0.1662
Mander et al. [13]	1988	$\dfrac{f'_{cc}}{f'_{co}} = -1.254 + 2.254\sqrt{1 + 7.940\dfrac{f_l}{f'_{co}} - 2\dfrac{f_l}{f'_{co}}}$	0.4710	0.1971
Wu and Zhou[*] [17]	2010	$\dfrac{f'_{cc}}{f'_{co}} = \sqrt{1 + (\dfrac{16.7}{f'^{0.42}_{co}} - \dfrac{f'^{0.42}_{co}}{16.7})\dfrac{f_l}{f'_{co}} + \dfrac{f_l}{f'_{co}}}$	0.5077	0.1585
Bing et al. [14]	2001	$\dfrac{f'_{cc}}{f'_{co}} = -0.413 + 1.413\sqrt{1 + 11.4\dfrac{f_l}{f'_{co}} - 2\dfrac{f_l}{f'_{co}}}$	0.5848	0.1576
Hales et al. [16]	2017	$\dfrac{f'_{cc}}{f'_{co}} = -3.373 + 4.373\sqrt{1 + 2.134\dfrac{f_l}{f'_{co}} - 2\dfrac{f_l}{f'_{co}}}$	0.6943	0.1881
Afifi et al. [15]	2015	$\dfrac{f'_{cc}}{f'_{co}} = 0.850 + \sqrt{0.17 + 6.43\dfrac{f_l}{f'_{co}} - 2\dfrac{f_l}{f'_{co}}}$	0.9057	0.2255

Table 4. Comparison of non-plasticity-based models.

Model	Year	Formula	RMSE	AAE
Sadeghian and Fam [26]	2015	$\dfrac{f'_{cc}}{f'_{co}} = 1 + (2.77\rho_K^{0.77} - 0.07)\rho_\varepsilon^{0.91}$	0.3603	0.1246
Lam and Teng [25]	2003	$\dfrac{f'_{cc}}{f'_{co}} = 1 + 3.3\dfrac{f_l}{f'_{co}}$	0.3882	0.1244
Teng et al. [24]	2009	$\dfrac{f'_{cc}}{f'_{co}} = 1 + 3.5(\rho_K - 0.01)\rho_\varepsilon$	0.4203	0.1264
Toutanji [65]	1999	$\dfrac{f'_{cc}}{f'_{co}} = 1 + 3.5\left(\dfrac{f_l}{f'_{co}}\right)^{0.85}$	0.4339	0.1799
Fallah Pour et al. [92]	2018	$\dfrac{f'_{cc}}{f'_{co}} = 1 + (2.5 - 0.01f'_{co})\dfrac{f_l}{f'_{co}}$	0.5528	0.1854
Rousakis et al. [91]	2012	$\dfrac{f'_{cc}}{f'_{co}} = 1 + (\rho_f E_f/f'_{co})(\alpha E_f 10^{-6}/E_{\mu f} + \beta)$	0.6601	0.1770
Mirmiran and Shahawy [23]	1997	$\dfrac{f'_{cc}}{f'_{co}} = 1 + 4.269\dfrac{f_l^{0.587}}{f'_{co}}$	0.8106	0.2437

Note: $\rho_K = \dfrac{2E_f t}{(f'_{co}/\varepsilon_{co})D}$; $\rho_\varepsilon = \dfrac{\varepsilon_{hr}}{\varepsilon_{co}}$; $\rho_f = \dfrac{4t}{D}$; $\varepsilon_{co} = 9.37 \times 10^{-4}\sqrt[4]{f'_{co}}$; t = thickness of FRP wrap; E_f = modulus of elasticity of FRP wrap; ε_{hr} = hoop rupture strain of FRP wrap; D = dimeter of concrete column; and ε_{co} = strain of unconfined concrete corresponding to f'_{co}; α = -0.336 and β = 0.0223 for FRP wraps; $E_{f\mu}$ = 10 MPa which is given for units' compliance.

Table 5. Database of parameters compiled out of 200 experimental full stress-strain curves from the literature.

No.	Source of data	Year	FRP	D (mm)	t_f (mm)	E_f (GPa)	f'_{co} (MPa)	f'_{cc} (MPa)	f'_{cc} / f'_{co}	$E_L{}^*$ (GPa)	$E_1{}^*$ (GPa)	$E_2{}^*$ (GPa)	$f_o{}^*$ (MPa)	f_o / f'_{co}	E_2/E_1 (%)
1	Xiao and Wu [53]	2000	CFRP	152	0.38	105	33.7	47.9	1.42	0.53	27.04	1.27	32.6	0.97	4.70
2	Xiao and Wu [53]	2000	CFRP	152	0.38	105	33.7	49.7	1.47	0.53	27.44	1.31	33.6	1.00	4.77
3	Xiao and Wu [53]	2000	CFRP	152	0.38	105	33.7	49.4	1.47	0.53	26.93	1.21	33.7	1.00	4.49
4	Xiao and Wu [53]	2000	CFRP	152	0.76	105	33.7	64.6	1.92	1.05	23.13	1.76	35.5	1.05	7.61
5	Xiao and Wu [53]	2000	CFRP	152	0.76	105	33.7	75.2	2.23	1.05	19.82	1.59	39.1	1.16	8.02
6	Xiao and Wu [53]	2000	CFRP	152	0.76	105	33.7	71.8	2.13	1.05	22.08	1.57	38.2	1.13	7.11
7	Xiao and Wu [53]	2000	CFRP	152	1.14	105	33.7	82.9	2.46	1.58	19.56	1.74	40.1	1.19	8.90
8	Xiao and Wu [53]	2000	CFRP	152	1.14	105	33.7	95.4	2.83	1.58	21.14	1.77	41.8	1.24	8.37
9	Xiao and Wu [53]	2000	CFRP	152	0.76	105	43.8	84.0	1.92	1.05	28.72	2.23	49.7	1.13	7.76
10	Xiao and Wu [53]	2000	CFRP	152	0.76	105	43.8	79.2	1.81	1.05	28.50	2.14	49.8	1.14	7.51
11	Xiao and Wu [53]	2000	CFRP	152	0.76	105	43.8	85.0	1.94	1.05	26.16	2.03	52.5	1.20	7.76
12	Xiao and Wu [53]	2000	CFRP	152	1.14	105	43.8	96.5	2.20	1.58	22.75	2.55	52.9	1.21	11.21
13	Xiao and Wu [53]	2000	CFRP	152	1.14	105	43.8	92.6	2.11	1.58	24.88	2.47	51.8	1.18	9.93
14	Xiao and Wu [53]	2000	CFRP	152	1.14	105	43.8	94.0	2.15	1.58	24.85	2.51	52.0	1.19	10.10
15	Xiao and Wu [53]	2000	CFRP	152	1.14	105	55.2	106.5	1.93	1.58	33.55	3.28	64.0	1.16	9.78
16	Xiao and Wu [53]	2000	CFRP	152	1.14	105	55.2	108.0	1.96	1.58	28.76	3.00	66.9	1.21	10.43
17	Xiao and Wu [53]	2000	CFRP	152	1.14	105	55.2	103.3	1.87	1.58	31.28	4.09	57.5	1.04	13.08
18	Lam and Teng [93]	2004	CFRP	152	0.17	258.8	35.9	50.4	1.40	0.56	30.47	1.36	33.9	0.94	4.46
19	Lam and Teng [93]	2004	CFRP	152	0.17	258.8	35.9	47.2	1.31	0.56	26.51	1.20	34.1	0.95	4.53
20	Lam and Teng [93]	2004	CFRP	152	0.17	258.8	35.9	53.2	1.48	0.56	24.92	1.46	34.6	0.96	5.86
21	Lam and Teng [93]	2004	CFRP	152	0.33	258.8	35.9	68.7	1.91	1.12	27.50	1.91	37.2	1.04	6.95
22	Lam and Teng [93]	2004	CFRP	152	0.33	258.8	35.9	69.9	1.95	1.12	24.58	1.66	37.8	1.05	6.75
23	Lam and Teng [93]	2004	CFRP	152	0.33	258.8	35.9	71.6	1.99	1.12	21.91	2.00	37.2	1.04	9.13
24	Lam and Teng [93]	2004	CFRP	152	0.50	258.8	34.3	82.6	2.41	1.69	22.55	2.34	35.6	1.04	10.38
25	Lam and Teng [93]	2004	CFRP	152	0.50	258.8	34.3	90.4	2.64	1.69	21.57	2.18	36.6	1.07	10.11
26	Lam and Teng [93]	2004	CFRP	152	0.50	258.8	34.3	97.3	2.84	1.69	25.73	2.41	36.4	1.06	9.37
27	Lam and Teng [93]	2004	GFRP	152	1.27	22.46	38.5	51.9	1.35	0.38	31.73	1.08	38.1	0.99	3.40
28	Lam and Teng [93]	2004	GFRP	152	1.27	22.46	38.5	58.3	1.51	0.38	25.92	1.01	43.7	1.14	3.90
29	Lam and Teng [93]	2004	GFRP	152	2.54	22.46	38.5	75.7	1.97	0.75	18.28	1.38	42.9	1.11	7.55
30	Lam and Teng [93]	2004	GFRP	152	2.54	22.46	38.5	77.3	2.01	0.75	24.27	1.53	44.2	1.15	6.30

No.	Author	Year	FRP												
31	Rousakis and Tepfers [94]	2004	CFRP	150	0.17	377	25.2	41.6	1.65	0.85	10.93	1.39	22.3	0.88	12.72
32	Rousakis and Tepfers [94]	2004	CFRP	150	0.17	377	25.2	38.8	1.54	0.85	13.43	1.72	20.0	0.79	12.81
33	Rousakis and Tepfers [94]	2004	CFRP	150	0.34	377	25.2	55.9	2.22	1.71	11.06	1.65	21.8	0.87	14.92
34	Rousakis and Tepfers [94]	2004	CFRP	150	0.51	377	25.2	67.0	2.66	2.56	10.95	1.78	24.0	0.95	16.26
35	Rousakis and Tepfers [94]	2004	CFRP	150	0.51	377	25.2	67.3	2.67	2.56	9.64	1.94	21.2	0.84	20.12
36	Rousakis and Tepfers [94]	2004	CFRP	150	0.17	377	51.8	78.7	1.52	0.85	26.99	3.43	53.3	1.03	12.71
37	Rousakis and Tepfers [94]	2004	CFRP	150	0.17	377	51.8	72.8	1.41	0.85	27.46	3.85	48.5	0.94	14.02
38	Rousakis and Tepfers [94]	2004	CFRP	150	0.34	377	51.8	95.4	1.84	1.71	26.25	4.57	47.9	0.92	17.41
39	Rousakis and Tepfers [94]	2004	CFRP	150	0.34	377	51.8	90.7	1.75	1.71	25.36	3.36	57.4	1.11	13.25
40	Rousakis and Tepfers [94]	2004	CFRP	150	0.51	377	51.8	110.5	2.13	2.56	25.85	4.29	55.8	1.08	16.60
41	Rousakis and Tepfers [94]	2004	CFRP	150	0.51	377	51.8	103.6	2.00	2.56	23.00	3.94	57.0	1.10	17.13
42	Rousakis and Tepfers [94]	2004	CFRP	150	0.85	377	51.8	126.7	2.45	4.27	28.35	4.51	59.6	1.15	15.91
43	Berthet et al. [95]	2005	CFRP	160	0.17	230	25.0	42.8	1.71	0.47	25.79	1.21	26.3	1.05	4.69
44	Berthet et al. [95]	2005	CFRP	160	0.33	230	25.0	55.2	2.21	0.95	19.87	1.48	32.2	1.29	7.45
45	Berthet et al. [95]	2005	CFRP	160	0.11	230	40.1	50.8	1.27	0.32	33.48	1.03	43.9	1.09	3.08
46	Berthet et al. [95]	2005	CFRP	160	0.17	230	40.1	53.7	1.34	0.47	36.83	1.40	45.3	1.13	3.80
47	Berthet et al. [95]	2005	CFRP	160	0.22	230	40.1	59.7	1.49	0.63	31.97	1.72	47.6	1.19	5.38
48	Berthet et al. [95]	2005	CFRP	160	0.44	230	40.1	91.6	2.28	1.27	31.70	2.73	53.9	1.34	8.61
49	Berthet et al. [95]	2005	CFRP	160	0.99	230	40.1	142.4	3.55	2.85	25.31	3.16	65.7	1.64	12.49
50	Berthet et al. [95]	2005	CFRP	160	1.32	230	40.1	166.3	4.15	3.80	31.24	3.81	66.0	1.65	12.20
51	Berthet et al. [95]	2005	CFRP	160	0.33	230	52.0	82.8	1.59	0.95	54.70	2.53	65.7	1.26	4.63
52	Berthet et al. [95]	2005	CFRP	160	0.66	230	52.0	108.1	2.08	1.90	48.61	3.31	72.0	1.38	6.81
53	Berthet et al. [95]	2005	CFRP	70	0.33	230	112.6	141.1	1.25	2.17	58.50	4.09	120.8	1.07	6.99
54	Berthet et al. [95]	2005	CFRP	70	0.82	230	112.6	189.5	1.68	5.39	66.25	5.55	142.5	1.27	8.38
55	Berthet et al. [95]	2005	CFRP	70	0.99	230	169.7	296.4	1.75	6.51	60.05	13.56	158.3	0.93	22.58
56	Berthet et al. [95]	2005	GFRP	160	0.33	74	25.0	42.8	1.71	0.31	25.42	0.92	27.6	1.10	3.62
57	Lam et al. [96]	2006	CFRP	152	0.17	250	41.1	57.0	1.39	0.54	26.68	1.51	39.0	0.95	5.66
58	Lam et al. [96]	2006	CFRP	152	0.17	250	41.1	55.4	1.35	0.54	30.83	1.54	38.5	0.94	5.00
59	Lam et al. [96]	2006	CFRP	152	0.33	250	38.9	79.1	2.03	1.09	28.87	2.00	38.6	0.99	6.93
60	Almusallam [97]	2007	GFRP	150	3.90	27	47.7	100.1	2.10	1.40	24.61	1.90	48.8	1.02	7.72
61	Almusallam [97]	2007	GFRP	150	3.90	27	50.8	90.8	1.79	1.40	28.90	2.00	51.7	1.02	6.92
62	Almusallam [97]	2007	GFRP	150	3.90	27	60.0	99.6	1.66	1.40	31.36	2.42	61.4	1.02	7.72
63	Almusallam [97]	2007	GFRP	150	3.90	27	90.3	110.0	1.22	1.40	48.56	1.81	94.4	1.05	3.73
64	Jiang and Teng [37]	2007	GFRP	152	0.17	80.1	33.1	42.4	1.28	0.18	18.62	0.46	36.7	1.11	2.47

65	Jiang and Teng [37]	2007	GFRP	152	0.17	80.1	33.1	41.6	1.26	0.18	21.44	0.54	35.1	1.06	2.52
66	Jiang and Teng [37]	2007	GFRP	152	0.34	80.1	45.9	52.8	1.15	0.36	33.29	0.47	47.0	1.02	1.41
67	Jiang and Teng [37]	2007	GFRP	152	0.34	80.1	45.9	55.2	1.20	0.36	34.11	0.59	47.5	1.03	1.73
68	Jiang and Teng [37]	2007	GFRP	152	0.51	80.1	45.9	64.6	1.41	0.54	23.06	1.03	49.3	1.07	4.47
69	Jiang and Teng [37]	2007	GFRP	152	0.51	80.1	45.9	65.9	1.44	0.54	17.63	0.79	50.9	1.11	4.48
70	Jiang and Teng [37]	2007	CFRP	152	0.68	240.7	38.0	110.1	2.90	2.15	17.48	2.22	55.9	1.47	12.70
71	Jiang and Teng [37]	2007	CFRP	152	0.68	240.7	38.0	107.4	2.83	2.15	20.09	2.36	48.7	1.28	11.75
72	Jiang and Teng [37]	2007	CFRP	152	1.02	240.7	38.0	129.0	3.39	3.23	21.66	2.70	56.1	1.48	12.47
73	Jiang and Teng [37]	2007	CFRP	152	1.02	240.7	38.0	135.7	3.57	3.23	16.83	2.63	55.0	1.45	15.63
74	Jiang and Teng [37]	2007	CFRP	152	1.36	240.7	38.0	161.3	4.24	4.31	19.53	2.79	59.7	1.57	14.29
75	Jiang and Teng [37]	2007	CFRP	152	1.36	240.7	38.0	158.5	4.17	4.31	14.69	2.77	61.1	1.61	18.86
76	Jiang and Teng [37]	2007	CFRP	152	0.11	260	37.7	48.5	1.29	0.38	27.59	1.09	38.9	1.03	3.95
77	Jiang and Teng [37]	2007	CFRP	152	0.11	260	37.7	50.3	1.33	0.38	27.39	1.32	38.3	1.02	4.82
78	Jiang and Teng [37]	2007	CFRP	152	0.11	260	44.2	48.1	1.09	0.38	27.64	1.15	40.2	0.91	4.16
79	Jiang and Teng [37]	2007	CFRP	152	0.11	260	44.2	51.1	1.16	0.38	30.25	0.91	43.1	0.98	3.01
80	Jiang and Teng [37]	2007	CFRP	152	0.22	260	44.2	65.7	1.49	0.75	30.07	1.87	43.9	0.99	6.22
81	Jiang and Teng [37]	2007	CFRP	152	0.22	260	44.2	62.9	1.42	0.75	27.00	2.12	41.0	0.93	7.85
82	Jiang and Teng [37]	2007	CFRP	152	0.33	260	47.6	82.7	1.74	1.13	31.99	2.52	50.2	1.05	7.88
83	Jiang and Teng [37]	2007	CFRP	152	0.33	260	47.6	85.5	1.80	1.13	31.83	2.13	51.5	1.08	6.69
84	Jiang and Teng [37]	2007	CFRP	152	0.33	260	47.6	85.5	1.80	1.13	28.92	2.09	49.4	1.04	7.23
85	Wang and Wu [98]	2008	CFRP	150	0.17	219	30.9	55.8	1.81	0.48	29.05	1.31	32.3	1.05	4.51
86	Wang and Wu [98]	2008	CFRP	150	0.17	219	52.1	67.9	1.30	0.48	34.96	1.57	49.6	0.95	4.49
87	Wang and Wu [98]	2008	CFRP	150	0.33	197	52.1	99.3	1.91	0.87	34.49	2.35	53.6	1.03	6.81
88	Benzaid et al. [99]	2010	CFRP	160	1.00	34	25.9	39.6	1.53	0.43	24.77	0.84	28.7	1.11	3.39
89	Benzaid et al. [99]	2010	CFRP	160	3.00	34	25.9	66.1	2.55	1.28	45.54	2.10	34.4	1.33	4.61
90	Benzaid et al. [99]	2010	CFRP	160	3.00	34	49.5	82.9	1.68	1.28	39.45	3.48	58.2	1.18	8.82
91	Benzaid et al. [99]	2010	CFRP	160	3.00	34	61.8	93.2	1.51	1.28	25.48	2.11	71.5	1.16	8.28
92	Cui and Sheikh [100]	2010	CFRP	152	1.00	84.6	48.1	80.9	1.68	1.11	31.95	2.40	47.2	0.98	7.51
93	Cui and Sheikh [100]	2010	CFRP	152	1.00	84.6	48.1	86.6	1.80	1.11	29.28	2.55	49.3	1.02	8.71
94	Cui and Sheikh [100]	2010	CFRP	152	2.00	84.6	48.1	109.4	2.27	2.23	28.26	2.99	50.2	1.04	10.58
95	Cui and Sheikh [100]	2010	CFRP	152	2.00	84.6	48.1	126.7	2.63	2.23	24.25	2.71	55.8	1.16	11.18
96	Cui and Sheikh [100]	2010	CFRP	152	3.00	84.6	48.1	162.7	3.38	3.34	29.15	3.42	58.7	1.22	11.73
97	Cui and Sheikh [100]	2010	CFRP	152	3.00	84.6	48.1	153.6	3.19	3.34	29.34	3.45	57.1	1.19	11.76
98	Cui and Sheikh [100]	2010	CFRP	152	1.00	84.6	48.1	84.2	1.75	1.11	32.48	2.26	50.6	1.05	6.96

99	Cui and Sheikh [100]	2010	CFRP	152	1.00	84.6	48.1	87.9	1.83	1.11	32.74	2.30	50.3	1.05	7.03
100	Cui and Sheikh [100]	2010	CFRP	152	2.00	84.6	48.1	123.3	2.56	2.23	29.07	2.92	55.1	1.15	10.04
101	Cui and Sheikh [100]	2010	CFRP	152	2.00	84.6	48.1	108.2	2.25	2.23	31.04	3.11	52.6	1.09	10.02
102	Cui and Sheikh [100]	2010	CFRP	152	3.00	84.6	48.1	156.5	3.25	3.34	30.10	3.30	55.8	1.16	10.96
103	Cui and Sheikh [100]	2010	CFRP	152	3.00	84.6	48.1	157.0	3.26	3.34	31.62	3.59	56.6	1.18	11.35
104	Cui and Sheikh [100]	2010	CFRP	152	1.00	84.6	79.9	105.3	1.32	1.11	53.05	2.59	86.3	1.08	4.88
105	Cui and Sheikh [100]	2010	CFRP	152	2.00	84.6	79.9	142.1	1.78	2.23	48.96	4.58	88.8	1.11	9.35
106	Cui and Sheikh [100]	2010	CFRP	152	2.00	84.6	79.9	140.8	1.76	2.23	44.66	4.92	89.6	1.12	11.02
107	Cui and Sheikh [100]	2010	CFRP	152	3.00	84.6	79.9	172.9	2.16	3.34	54.30	5.69	88.4	1.11	10.48
108	Cui and Sheikh [100]	2010	CFRP	152	3.00	84.6	79.9	181.8	2.28	3.34	51.54	5.80	94.8	1.19	11.25
109	Cui and Sheikh [100]	2010	CFRP	152	0.11	241.3	45.6	57.7	1.27	0.35	31.30	0.86	47.5	1.04	2.75
110	Cui and Sheikh [100]	2010	CFRP	152	0.11	241.3	45.6	55.4	1.21	0.35	36.41	0.86	44.1	0.97	2.36
111	Cui and Sheikh [100]	2010	CFRP	152	0.22	241.3	45.6	78.0	1.71	0.70	26.92	1.68	46.0	1.01	6.24
112	Cui and Sheikh [100]	2010	CFRP	152	0.22	241.3	45.6	86.8	1.90	0.70	28.08	1.79	48.8	1.07	6.37
113	Cui and Sheikh [100]	2010	CFRP	152	0.33	241.3	45.6	106.5	2.34	1.06	31.18	2.14	45.9	1.01	6.86
114	Cui and Sheikh [100]	2010	CFRP	152	0.33	241.3	45.6	106.0	2.32	1.06	32.22	2.20	48.2	1.06	6.83
115	Cui and Sheikh [100]	2010	CFRP	152	0.11	241.3	45.6	56.3	1.23	0.35	38.63	1.01	43.5	0.95	2.61
116	Cui and Sheikh [100]	2010	CFRP	152	0.11	241.3	45.6	58.8	1.29	0.35	38.72	1.31	44.2	0.97	3.38
117	Cui and Sheikh [100]	2010	CFRP	152	0.22	241.3	45.6	81.9	1.80	0.70	31.08	1.89	46.9	1.03	6.08
118	Cui and Sheikh [100]	2010	CFRP	152	0.22	241.3	45.6	82.8	1.82	0.70	38.69	1.66	46.7	1.02	4.29
119	Cui and Sheikh [100]	2010	CFRP	152	0.33	241.3	45.6	107.3	2.35	1.06	32.44	2.16	47.3	1.04	6.66
120	Cui and Sheikh [100]	2010	CFRP	152	0.33	241.3	45.6	108.6	2.38	1.06	32.96	2.21	48.3	1.06	6.71
121	Cui and Sheikh [100]	2010	CFRP	152	0.16	437.5	45.7	67.5	1.48	0.94	39.02	2.40	41.8	0.91	6.15
122	Cui and Sheikh [100]	2010	CFRP	152	0.16	437.5	45.7	64.1	1.40	0.94	42.57	2.47	39.2	0.86	5.80
123	Cui and Sheikh [100]	2010	CFRP	152	0.33	437.5	45.7	84.2	1.84	1.88	33.43	3.32	40.6	0.89	9.93
124	Cui and Sheikh [100]	2010	CFRP	152	0.33	437.5	45.7	83.1	1.82	1.88	32.97	3.33	43.1	0.94	10.10
125	Cui and Sheikh [100]	2010	CFRP	152	0.49	437.5	45.7	99.7	2.18	2.81	32.23	3.53	45.1	0.99	10.95
126	Cui and Sheikh [100]	2010	CFRP	152	0.49	437.5	45.7	94.9	2.08	2.81	36.01	3.67	42.8	0.94	10.19
127	Cui and Sheikh [100]	2010	CFRP	152	0.16	437.5	45.7	65.8	1.44	0.94	36.59	2.49	42.1	0.92	6.81
128	Cui and Sheikh [100]	2010	CFRP	152	0.16	437.5	45.7	65.9	1.44	0.94	35.49	2.41	41.7	0.91	6.79
129	Cui and Sheikh [100]	2010	CFRP	152	0.33	437.5	45.7	88.1	1.93	1.88	38.43	3.30	41.2	0.90	8.59
130	Cui and Sheikh [100]	2010	CFRP	152	0.33	437.5	45.7	82.0	1.79	1.88	33.51	3.33	42.2	0.92	9.94
131	Cui and Sheikh [100]	2010	CFRP	152	0.65	437.5	45.7	103.2	2.26	3.75	33.70	3.94	43.7	0.96	11.69
132	Cui and Sheikh [100]	2010	CFRP	152	0.65	437.5	45.7	105.6	2.31	3.75	35.01	3.31	45.0	0.98	9.45

133	Cui and Sheikh [100]	2010	CFRP	152	0.33	437.5	85.7	117.7	1.37	1.88	45.57	3.70	90.4	1.05	8.12
134	Cui and Sheikh [100]	2010	CFRP	152	0.33	437.5	85.7	117.5	1.37	1.88	42.86	4.45	89.9	1.05	10.38
135	Cui and Sheikh [100]	2010	CFRP	152	0.65	437.5	85.7	161.6	1.89	3.75	44.32	7.53	86.4	1.01	16.99
136	Cui and Sheikh [100]	2010	CFRP	152	0.65	437.5	85.7	162.6	1.90	3.75	46.49	7.16	94.8	1.11	15.40
137	Cui and Sheikh [100]	2010	GFRP	152	1.25	21.47	47.7	59.1	1.24	0.35	59.65	1.30	42.8	0.90	2.18
138	Cui and Sheikh [100]	2010	GFRP	152	1.25	21.47	47.7	59.8	1.25	0.35	51.96	1.49	43.0	0.90	2.87
139	Cui and Sheikh [100]	2010	GFRP	152	2.50	21.47	47.7	88.9	1.86	0.71	42.60	1.99	47.3	0.99	4.67
140	Cui and Sheikh [100]	2010	GFRP	152	2.50	21.47	47.7	88.0	1.84	0.71	36.34	1.92	47.2	0.99	5.28
141	Cui and Sheikh [100]	2010	GFRP	152	3.75	21.47	47.7	113.2	2.37	1.06	31.03	2.24	52.3	1.10	7.22
142	Cui and Sheikh [100]	2010	GFRP	152	3.75	21.47	47.7	112.5	2.36	1.06	27.13	2.20	52.0	1.09	8.11
143	Cui and Sheikh [100]	2010	GFRP	152	1.25	21.47	47.7	63.4	1.33	0.35	36.99	1.10	47.0	0.99	2.97
144	Cui and Sheikh [100]	2010	GFRP	152	1.25	21.47	47.7	62.4	1.31	0.35	49.53	1.14	47.7	1.00	2.30
145	Cui and Sheikh [100]	2010	GFRP	152	2.50	21.47	47.7	89.7	1.88	0.71	40.00	1.98	47.9	1.00	4.95
146	Cui and Sheikh [100]	2010	GFRP	152	2.50	21.47	47.7	88.3	1.85	0.71	34.73	2.01	48.8	1.02	5.79
147	Cui and Sheikh [100]	2010	GFRP	152	3.75	21.47	47.7	108.0	2.26	1.06	32.03	2.20	52.5	1.10	6.87
148	Dai et al. [101]	2011	AFRP	152	0.17	115.2	39.2	61.4	1.57	0.26	16.70	0.85	41.8	1.07	5.09
149	Dai et al. [101]	2011	AFRP	152	0.17	115.2	39.2	62.7	1.60	0.26	13.54	0.83	43.8	1.12	6.13
150	Dai et al. [101]	2011	AFRP	152	0.17	115.2	39.2	55.8	1.42	0.26	14.87	1.00	35.3	0.90	6.72
151	Dai et al. [101]	2011	AFRP	152	0.34	115.2	39.2	90.1	2.30	0.51	16.26	1.22	47.3	1.21	7.50
152	Dai et al. [101]	2011	AFRP	152	0.34	115.2	39.2	88.3	2.25	0.51	19.04	1.35	43.0	1.10	7.09
153	Dai et al. [101]	2011	AFRP	152	0.34	115.2	39.2	83.3	2.13	0.51	11.70	1.19	40.6	1.04	10.17
154	Dai et al. [101]	2011	AFRP	152	0.51	115.2	39.2	113.2	2.89	0.77	15.30	1.51	52.6	1.34	9.87
155	Dai et al. [101]	2011	AFRP	152	0.51	115.2	39.2	116.3	2.97	0.77	11.68	1.42	53.8	1.37	12.16
156	Dai et al. [101]	2011	AFRP	152	0.51	115.2	39.2	118	3.01	0.77	12.28	1.38	53.4	1.36	11.24
157	Wang et al. [102]	2012	CFRP	204	0.17	244	24.5	46.1	1.88	0.40	13.22	0.77	27.8	1.13	5.82
158	Wang et al. [102]	2012	CFRP	204	0.33	244	24.5	65.2	2.66	0.80	13.59	1.03	29.2	1.19	7.58
159	Lim and Ozbakkaloglu [103]	2014	AFRP	150	0.20	128.5	29.6	52.5	1.77	0.34	29.30	1.03	31.4	1.06	3.52
160	Lim and Ozbakkaloglu [103]	2014	AFRP	150	0.20	128.5	29.6	50.3	1.70	0.34	25.00	1.02	30.6	1.03	4.08
161	Lim and Ozbakkaloglu [103]	2014	AFRP	150	0.20	128.5	29.6	50.5	1.71	0.34	28.87	0.93	32.2	1.09	3.22
162	Lim and Ozbakkaloglu [103]	2014	CFRP	150	0.17	236	29.6	57.3	1.94	0.52	32.13	1.18	36.1	1.22	3.67
163	Lim and Ozbakkaloglu [103]	2014	CFRP	150	0.17	236	29.6	60.4	2.04	0.52	27.86	1.25	35.9	1.21	4.49

164	Lim and Ozbakkaloglu [103]	2014	CFRP	150	0.17	236	29.6	61.2	2.07	0.52	31.65	1.18	35.2	1.19	3.73
165	Lim and Ozbakkaloglu [103]	2014	GFRP	150	0.20	95.3	29.6	50.8	1.72	0.25	30.38	0.87	35.8	1.21	2.86
166	Lim and Ozbakkaloglu [103]	2014	GFRP	150	0.20	95.3	29.6	46.6	1.57	0.25	26.08	0.87	33.8	1.14	3.34
167	Lim and Ozbakkaloglu [103]	2014	GFRP	150	0.20	95.3	29.6	49.4	1.67	0.25	24.38	0.76	34.9	1.18	3.12
168	Lim and Ozbakkaloglu [103]	2014	AFRP	150	0.40	128.5	49.6	83.1	1.68	0.69	33.90	1.34	49.6	1.00	3.95
169	Lim and Ozbakkaloglu [103]	2014	AFRP	150	0.40	128.5	49.6	87.2	1.76	0.69	24.50	1.55	53.0	1.07	6.33
170	Lim and Ozbakkaloglu [103]	2014	AFRP	150	0.40	128.5	49.6	84	1.69	0.69	35.15	1.26	51.1	1.03	3.58
171	Lim and Ozbakkaloglu [103]	2014	CFRP	150	0.33	236	49.6	98	1.98	1.04	37.96	1.92	52.5	1.06	5.06
172	Lim and Ozbakkaloglu [103]	2014	CFRP	150	0.33	236	49.6	95.3	1.92	1.04	43.99	2.01	54.0	1.09	4.57
173	Lim and Ozbakkaloglu [103]	2014	CFRP	150	0.33	236	49.6	100.3	2.02	1.04	38.93	2.11	58.2	1.17	5.42
174	Lim and Ozbakkaloglu [103]	2014	GFRP	150	0.40	95.3	49.6	78.3	1.58	0.51	44.20	1.33	55.3	1.11	3.01
175	Lim and Ozbakkaloglu [103]	2014	GFRP	150	0.40	95.3	49.6	75.6	1.52	0.51	34.78	1.15	55.6	1.12	3.31
176	Lim and Ozbakkaloglu [103]	2014	GFRP	150	0.40	95.3	49.6	71.4	1.44	0.51	43.93	1.20	55.5	1.12	2.73
177	Lim and Ozbakkaloglu [103]	2014	GFRP	150	0.60	95.3	74.1	90.8	1.23	0.76	51.91	1.66	81.8	1.10	3.20
178	Lim and Ozbakkaloglu [103]	2014	GFRP	150	0.60	95.3	74.1	91.8	1.24	0.76	41.65	1.53	74.0	1.00	3.67
179	Lim and Ozbakkaloglu [104]	2014	AFRP	150	1.20	128.5	85.7	166.2	1.94	2.06	36.49	2.89	107.0	1.25	7.92
180	Lim and Ozbakkaloglu [104]	2014	AFRP	150	1.20	128.5	85.7	168	1.96	2.06	51.10	2.95	101.3	1.18	5.77
181	Lim and Ozbakkaloglu [104]	2014	AFRP	150	1.20	128.5	85.6	165.2	1.93	2.06	45.65	2.80	102.9	1.20	6.13
182	Lim and Ozbakkaloglu [104]	2014	AFRP	150	1.20	128.5	112.3	168.4	1.50	2.06	54.73	3.49	107.5	0.96	6.38
183	Lim and Ozbakkaloglu [104]	2014	GFRP	150	0.80	95.3	57.4	125.7	2.19	1.02	49.45	1.74	67.5	1.18	3.52
184	Lim and Ozbakkaloglu [104]	2014	GFRP	150	0.80	95.3	57.3	127.2	2.22	1.02	41.29	1.58	71.4	1.25	3.83
185	Lim and Ozbakkaloglu [104]	2014	GFRP	150	0.80	95.3	57.3	131.2	2.29	1.02	26.10	1.60	72.8	1.27	6.13
186	Lim and Ozbakkaloglu [104]	2015	AFRP	150	0.80	128.5	74.8	130.1	1.74	1.37	42.94	2.33	89.9	1.20	5.43

#	Reference	Year	Type												
187	Lim [105]	2015	AFRP	150	0.80	128.5	75.0	130.5	1.74	1.37	48.23	1.92	91.4	1.22	3.98
188	Lim [105]	2015	AFRP	150	0.80	128.5	74.9	139.3	1.86	1.37	42.50	2.19	91.8	1.23	5.15
189	Lim [105]	2015	GFRP	150	0.80	95.3	73.9	136.0	1.84	1.02	44.02	1.76	90.4	1.22	4.00
190	Lim [105]	2015	GFRP	150	0.80	95.3	74.2	138.7	1.87	1.02	38.41	1.76	90.5	1.22	4.58
191	Lim [105]	2015	GFRP	150	0.80	95.3	74.1	136.3	1.84	1.02	48.89	1.82	87.1	1.18	3.72
192	Lim [105]	2015	GFRP	150	0.40	95.3	34.8	78.1	2.25	0.51	30.16	1.19	40.3	1.16	3.95
193	Lim [105]	2015	GFRP	150	0.40	95.3	34.7	76.3	2.20	0.51	27.67	1.10	39.4	1.14	3.98
194	Lim [105]	2015	GFRP	150	0.40	95.3	34.8	75.1	2.16	0.51	30.71	1.13	40.8	1.17	3.68
195	Fillmore and Sadeghian [84]	2018	BFRP	150	0.90	24.62	40.0	55.9	1.40	0.30	38.46	1.32	45.0	1.13	3.43
196	Fillmore and Sadeghian [84]	2018	BFRP	150	0.90	24.62	40.0	56.8	1.42	0.30	34.86	1.44	45.6	1.14	4.13
197	Fillmore and Sadeghian [84]	2018	BFRP	150	1.80	24.62	40.0	76.4	1.91	0.59	30.67	1.42	49.4	1.24	4.63
198	Fillmore and Sadeghian [84]	2018	BFRP	150	1.80	24.62	40.0	78.2	1.95	0.59	44.75	1.55	49.7	1.24	3.46
199	Fillmore and Sadeghian [84]	2018	BFRP	150	2.70	24.62	40.0	95.4	2.38	0.89	32.39	2.14	50.5	1.26	6.61
200	Fillmore and Sadeghian [84]	2018	BFRP	150	2.70	24.62	40.0	99.0	2.47	0.89	41.14	1.71	54.5	1.36	4.16
Mean				151	0.89	178.2	47.8	90.5	1.94	1.29	31.56	2.21	52.43	1.10	7.36
STD				11.6	0.9	122.5	18.4	36.7	0.6	1.05	10.7	1.4	20.6	0.14	3.9
COV(%)				8	105	69	38	41	30	82	34	64	40	13	53

Note: * The values are found in the current study; STD = standard deviation; COV = coefficient of variation.

Table 6. Performance comparison of the proposed axial stress-strain model against the models from the literature (sorted based on the lowest RMSE).

No.	Resource	Year	RMSE	AAE	MSE	SD
1	Current study	2020	6.17	0.0930	0.0185	0.1361
2	Fahmy and Wu [63]	2010	7.20	0.1021	0.0196	0.1320
3	Teng et al. [90]	2009	7.53	0.1036	0.0202	0.1282
4	Lam and Teng [25]	2003	8.13	0.1054	0.0209	0.1377
5	Yu and Teng [62]	2011	8.19	0.1192	0.0238	0.1287
6	Xiao and Wu [70]	2003	8.97	0.1132	0.0245	0.1466
7	Samaan et al. [21]	1998	13.48	0.1872	0.0483	0.1394
8	Saadatmanesh et al. [106]*	1994	16.55	0.2105	0.0688	0.2320
9	Youssef et al. [107]	2007	18.71	0.2166	0.0632	0.1490
10	Djafar-Henni and Kassoul [73]	2018	19.24	0.1928	0.0842	0.2894
11	Yan et al. [18]	2007	32.60	0.4394	0.2287	0.2489
12	Wu et al. [71]	2009	44.98	0.3987	0.2784	0.4413
13	Xiao and Wu [53]	2000	45.24	0.5768	1.0240	0.8686
14	Wu and Wang [72]	2010	48.94	0.4289	0.3251	0.4733
15	Fardis and Khalili [46]	1982	49.83	0.6904	0.5020	0.1648

* Saadatmanesh et al. [106] used Mander et al. [13] for confining pressure and Popovics [50] curve.

Table 7. Comparison of the ultimate confined strain.

Selected rupture strain	No.	Resource	Year	Formula	RMSE for $\frac{\varepsilon_{cc}}{\varepsilon_{co}}$	AAE for $\frac{\varepsilon_{cc}}{\varepsilon_{co}}$
Hoop rupture strain (ε_{hr}) used for the ultimate condition	1	Current study (Eq. 33)	2020	$\varepsilon_{cc} = \dfrac{f'_{cc} - f_o}{E_2}$	2.675	0.316
	2	Teng et al. [24]	2009	$\dfrac{\varepsilon_{cc}}{\varepsilon_{co}} = 1.75 + 12\rho_K \rho_\varepsilon^{1.45}$ $\rho_K = \dfrac{2E_f t_f}{(f'_{co}/\varepsilon_{co})D}$; $\rho_\varepsilon = \dfrac{\varepsilon_{hr}}{\varepsilon_{co}}$	3.46	0.361
	3	Pham and Hadi [87]	2013	$\varepsilon_{cc} = \varepsilon_{co} + \dfrac{4kt_f f_{fe}\varepsilon_{fe}}{D(f'_{co} + f'_{cc})}$ $\varepsilon_{co} = \left(-0.067f'_{co}{}^2 + 29.9f'_{co} + 1053\right) \times 10^{-6}$ $f_{fe} = E_f \varepsilon_{fe}$; $k = 7.6$	4.83	0.416
Effective rupture strain ($\varepsilon_{fe} = k_e \varepsilon_{fu}$) was used for the ultimate condition	4	Current study (Eq. 33)	2020	$\varepsilon_{cc} = \dfrac{f'_{cc} - f_o}{E_2}$	3.208	0.452
	5	Wu and Cao [89]	2017	$\dfrac{\varepsilon_{cc}}{\varepsilon_{co}} = 1.75 + 27.34\left(\dfrac{f_{30}}{f_{co}}\right)^{0.354}\left(\dfrac{E_L}{f_{co}}\right)^{-0.165}\dfrac{E_1}{E_{sec} + 1.75E_2}\left(\dfrac{\varepsilon_{fu}}{\varepsilon_{co}}\right)^{1.16}$ $E_2 = n_2(245.6f_{co}^{n1} + 0.6728E_L)$ $f_{30} = 30MPa$; $E_{sec} = f_{co}/\varepsilon_{co}$ $n_1 = 0.5$, $n_2 = 0.83$ for $f'_{co} \le 40MPa$ $n_1 = 0.2$, $n_2 = 1.73$ for $f'_{co} > 40MPa$	4.048	0.488
	6	Lim and Ozbakkaloglu [88]	2015	$\varepsilon_{cc} = \dfrac{\varepsilon_{hr}}{v_i\left[1 + \left(\dfrac{\varepsilon_{hr}}{v_i\varepsilon_{co}}\right)^n\right]^{1/n}} + 0.04\varepsilon_{hr}^{0.7}\left[1 + 21\left(\dfrac{f_l}{f'_{co}}\right)^{0.8}\right]$ $v_i = 8 \times 10^{-6}f'_{co}{}^2 + 0.0002f'_{co} + 0.138$ $\varepsilon_{co} = \left(-0.067f'_{co}{}^2 + 29.9f'_{co} + 1053\right) \times 10^{-6}$ $n = 1 + f'_{co}$ $\varepsilon_{hr} = k_e\varepsilon_{fu}$; $k_e = 0.9 - 2.3f'_{co} \times 10^{-3} - 0.75E_f \times 10^{-6}$	4.14	0.422

Note: For comparison of errors, all predicted values of ultimate confined strain (ε_{cc}) were normalized by the strain corresponding to the unconfined concrete strength ($\boldsymbol{\varepsilon_{co} = 9.37 \times 10^{-4}\sqrt[4]{f'_{co}}}$).
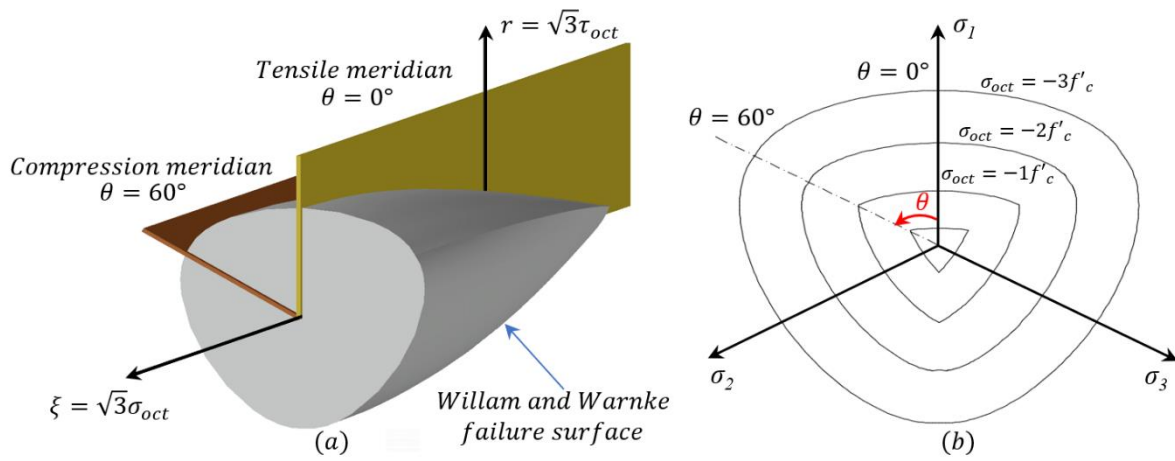
Fig. 1. Five-parameter plasticity model of Willam and Warnke [29]: (a) Three-dimensional scheme and(b) Schematic deviatoric sections.
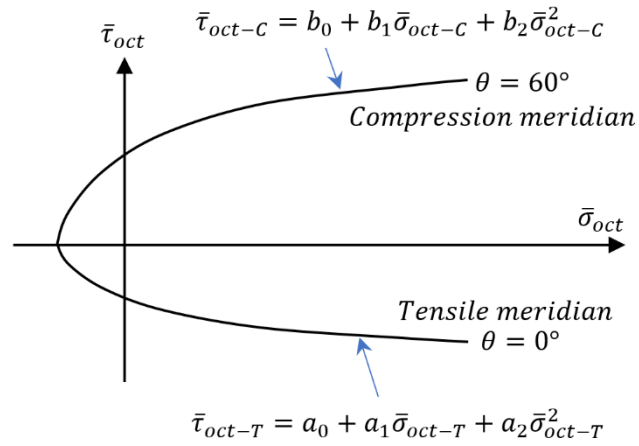
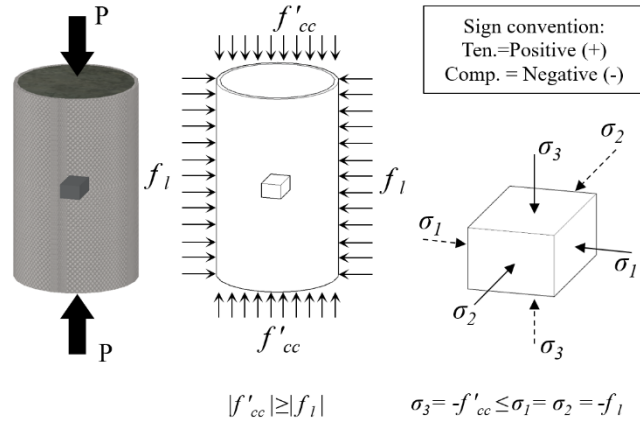**Fig. 2. Compression and tensile meridians.**

Fig. 3. Principal stresses in FRP-wrapped concrete column under pure compression.
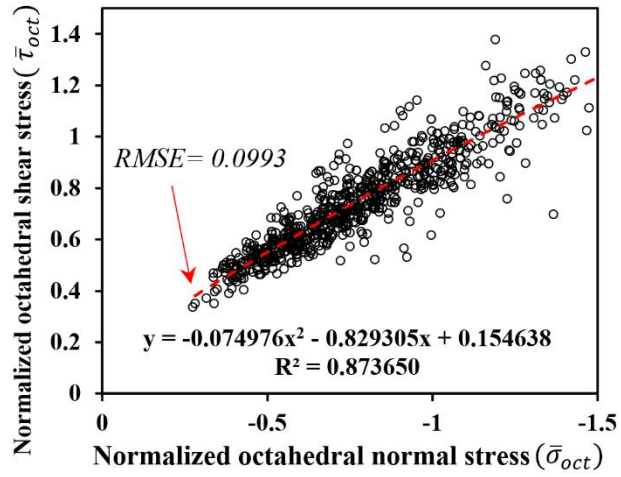
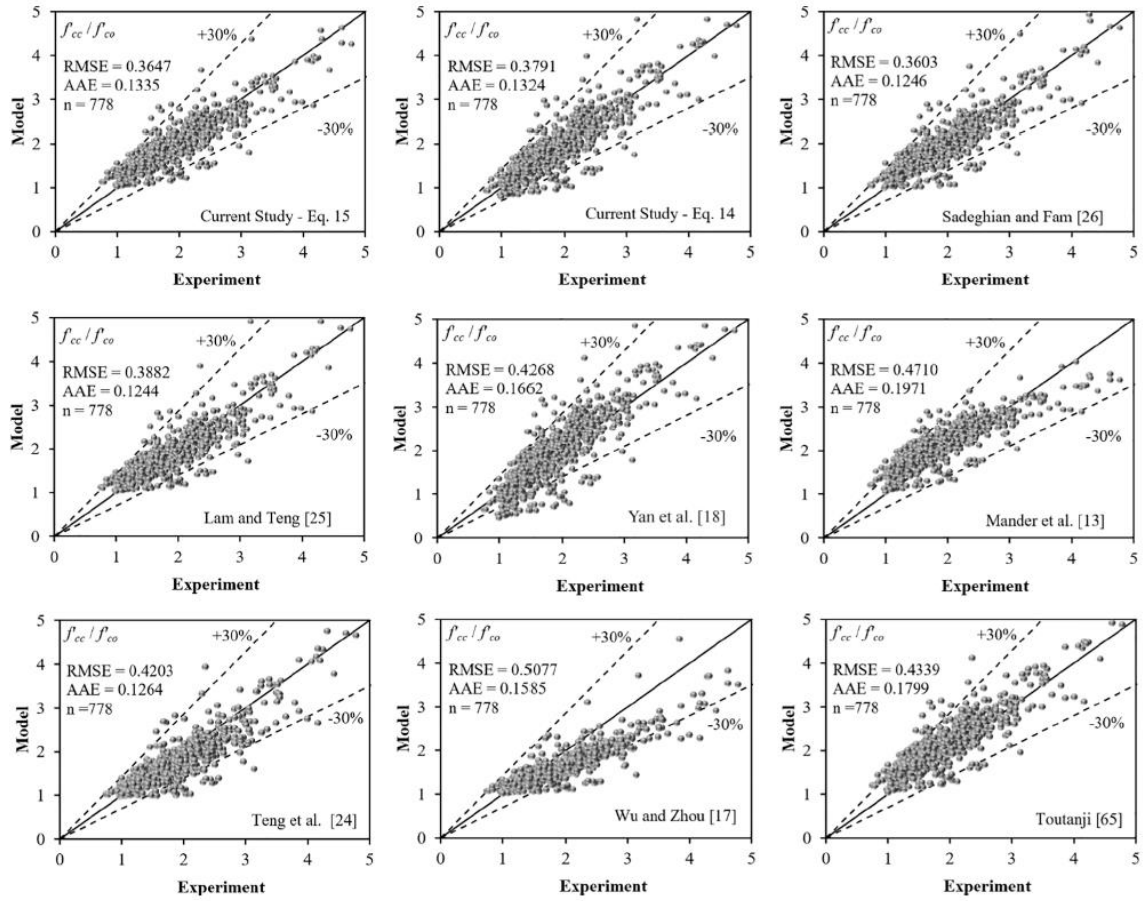**Fig. 4. Derivation of the best-fitted curve in octahedral space for compression meridian.**

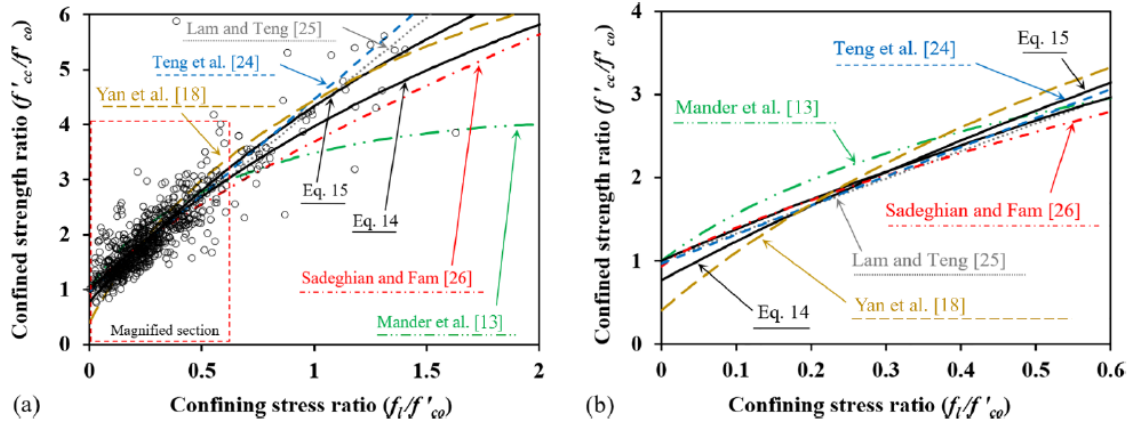**Fig. 5. Comparison of the predicted values and the experimental test results for strength.**

Fig. 6. Comparison of confined concrete equations: (a) database and (b) selected range.
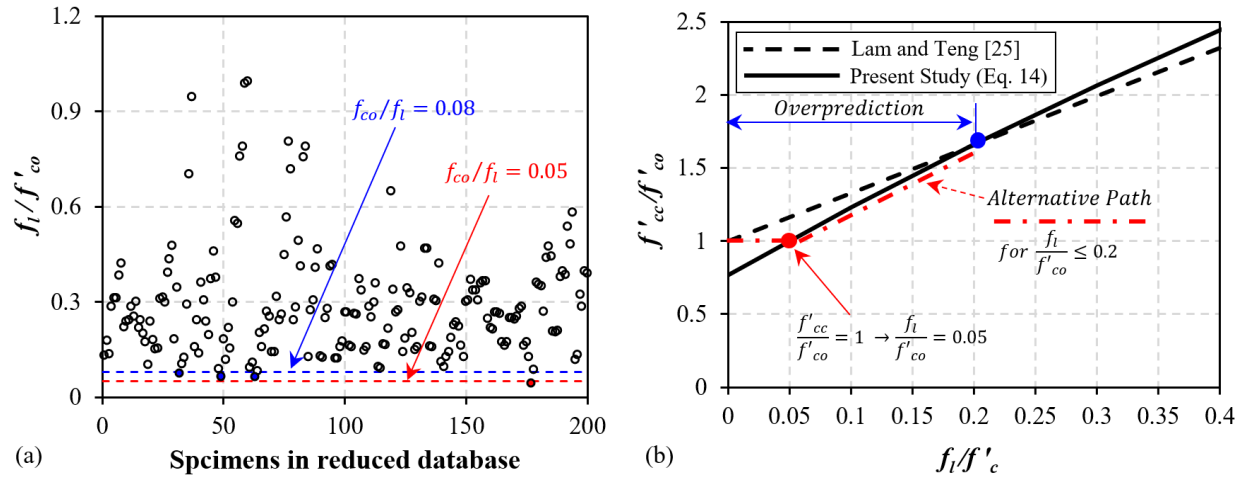
Fig. 7. Minimum required confinement limit: (a) reduced database and (b) comparison.
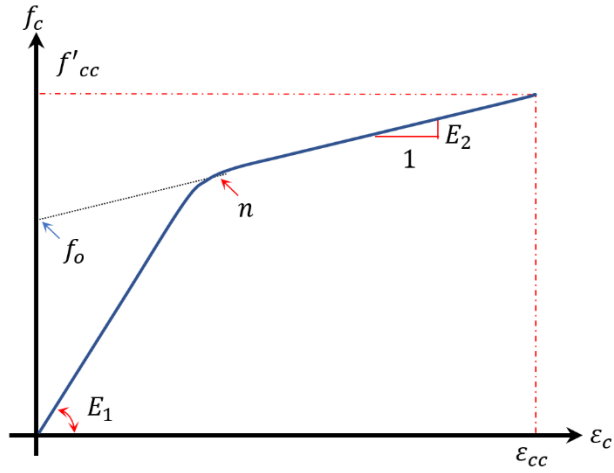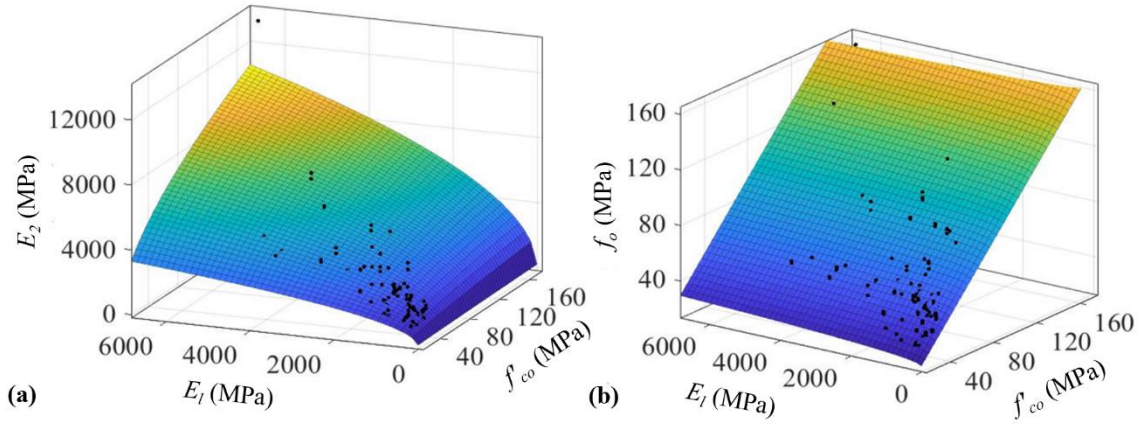
Fig. 8. Schematic Stress-Strain Curve Models.

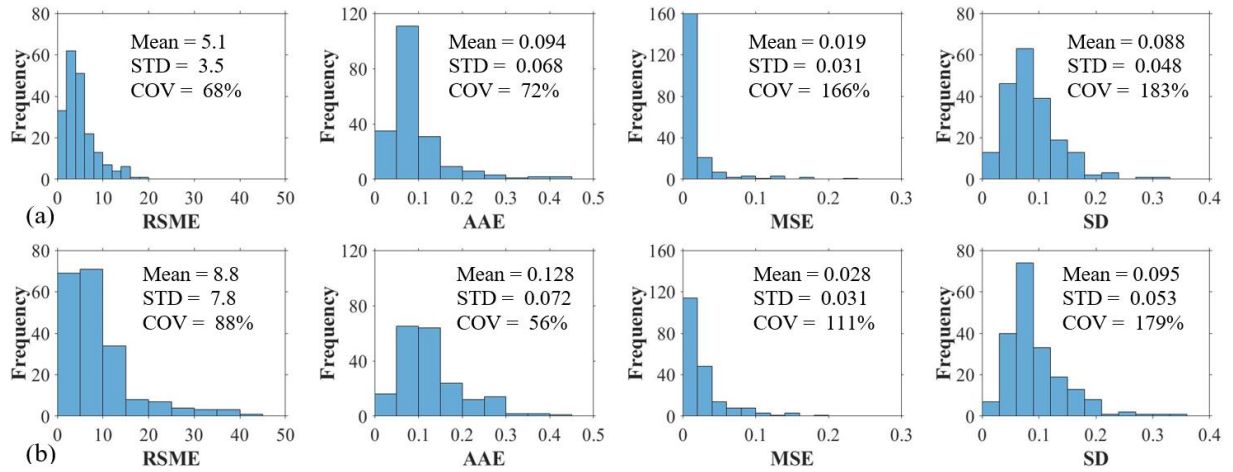**Fig. 9. Regression results for deriving equations for: (a) E_2 and (b) f_o.**

Fig. 10. Error distribution for axial stress-strain: (a) Current study and (b) Lam and Teng [25].
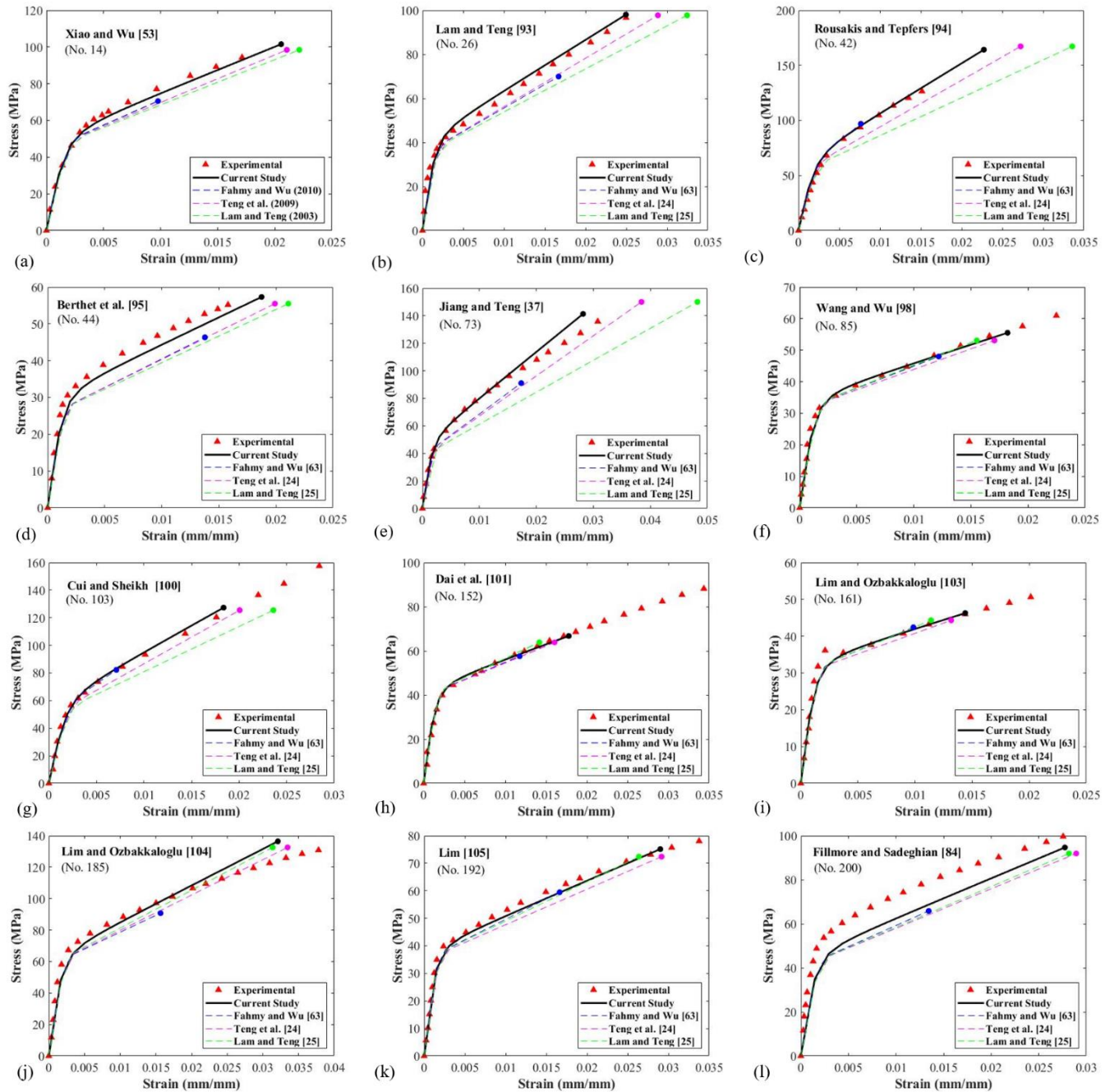
Fig. 11. Sample of axial stress-strain curves: (a) Xiao and Wu [53]; (b) Lam and Teng [93]; (c) Rousakis and Tepfers [94]; (d) Berthet et al. [95]; (e) Jiang and Teng [37]; (f) Wang and Wu [98]; (g) Cui and Sheikh [100]; (h) Dai et al. [101]; (i) Lim and Ozbakkaloglu [103]; (j) Lim and Ozbakkaloglu [104]; (k) Lim [105]; (l) Fillmore and Sadeghian [84].